1   **Trophic state assessment of global inland waters using a MODIS-**

2   **derived Forel-Ule index**

3   Shenglei Wang[a,b,c], Junsheng Li[a,b], Bing Zhang[a,b,*], Evangelos Spyrakos[c], Andrew N. Tyler[c], Qian

4   Shen[a], Fangfang Zhang[a], Tiit Kuster[d], Moritz K. Lehmann[e], Yanhong Wu[a], Dailiang Peng[a]

5   [a]*Key Laboratory of Digital Earth, Instituteof Remote Sensing and Digital Earth, Chinese Academy of*

6   *Sciences, Beijing100094, China*

7   [b]*University of Chinese Academy of Sciences, Beijing 100049, China*

8   [c]*Biological and Environmental Sciences, School of Natural Sciences, University of Stirling, Stirling,*

9   *United Kingdom*

10   [d]*Estonian Marine Institute, University of Tartu, Mäealuse 14, Tallinn, 12618, Estonia*

11   [e]*Environmental Research Institute, University of Waikato, Hamilton, New Zealand*

12   [*]*Corresponding author, e-mail address:* zb@radi.ac.cn

Abstract

14   Eutrophication of inland waters is considered a serious global environmental

15   problem. Satellite remote sensing (RS) has been established as an important source of

16   information to determine the trophic state of inland waters through the retrieval of

17   optically active water quality parameters such as chlorophyll-a (Chl-a). However, the

18   use of RS techniques for assessment of the trophic state of inland waters on a global

19   scale is hindered by the performance of retrieval algorithms over highly dynamic and

20   complex optical properties that characterize many of these systems. In this study, we

21   developed a new RS approach to assess the trophic state of global inland water bodies

22   based on Moderate Resolution Imaging Spectroradiometer (MODIS) imagery and the

23   Forel-Ule index (FUI). First, the FUI was calculated from MODIS data by dividing

24   natural water colour into 21 indices from dark blue to yellowish-brown. Then the

25   relationship between FUI and the trophic state index (TSI) was established based on in-

26   situ measurements and MODIS products. The water-leaving reflectance at 645 nm band

27   was employed to distinguish coloured dissolved organic matter (CDOM)-dominated

28   systems in the FUI-based trophic state assessment. Based on the analysis, the FUI-based

29   trophic state assessment method was developed and applied to assess the trophic states

30   of 2058 large inland water bodies (surface area > 25 km^2) distributed around the world

31   using MODIS data from the austral and boreal summers of 2012. Our results showed

32   that FUI can be retrieved from MODIS with a considerable accuracy (92.5%, R^2=0.92)

33   by comparing with concurrent in situ measurements over a wide range of lakes, and the

34   overall accuracy of the FUI-based trophic state assessment method is 80.0% ($R^2 = 0.75$)

35   validated by an independent dataset. Of the global large water bodies considered,

36   oligotrophic large lakes were found to be concentrated in plateau regions in central Asia

37   and southern South America, while eutrophic large lakes were concentrated in central

38   Africa, eastern Asia, and mid-northern and southeast North America.

1. Introduction

Eutrophication represents a serious water quality challenge around the world (Jones and Lee, 1982; Le et al., 2010; Smith, 2003; Vollenweider, 1981). This process is often associated with the rapid production of phytoplankton and other microorganisms, which have important impacts on aquatic ecology and the normal functioning of water bodies (Vollenweider and Kerekes, 1982). The trophic state of inland waters is typically categorized into three levels: oligotrophic, mesotrophic, and eutrophic. Since the 1960s, attempts have been made to quantitatively evaluate the trophic state of inland waters using both single-variable and multi-variable methods (Beeton and Edmondson, 1972; Bigham Stephens et al., 2015; Burns and Bryers, 2000; Forsberg and Ryding, 1980; Rodhe, 1969). Carlson (1977) introduced a numerical *Trophic State Index* (TSI) for inland waters based on algae biomass, which can be calculated using Secchi depth (SD), chlorophyll-a (Chl-a), or total phosphorus (TP). Many studies have used Chl-a, a pigment common to almost all photosynthetic organisms, as a proxy for algal biomass and therefore also as an indicator for the trophic state of aquatic systems (Carlson, 1991; Joniak et al., 2009; Sheela et al., 2011a). The Trophic Level Index (TLI), another commonly used numerical method, is calculated from the weighted sum of either three variables (Chl-a, TP, total nitrogen (TN)) or five variables with the addition of SD and chemical oxygen demand (COD) (Burns and Bryers, 2000; Burns et al., 1999; Jin and Tu, 1990; Verburg et al., 2010).

60   Collecting systematic observations on the ecological status of inland waters in

61   aquatic systems in inland waters remains a logistical and financial challenge which with

62   conventional in-situ approaches scales proportionately with increasing geographical

63   coverage (Härmä et al., 2001; Hu et al., 2010; McClain, 2009). However, satellite based

64   remote sensing (RS) offers a potentially significant source of information for large-

65   scale monitoring of water state variables (including water trophic state).

66   Eutrophication and increased productivity typically result in changes in the optical

67   properties of water; therefore, RS approaches have been employed for water trophic

68   state assessment (Baban, 1996; Papoutsa et al., 2014), in particular through the retrieval

69   of Chl-a concentrations (Chen, 2003; Duan et al., 2007; Matthews and Odermatt, 2015;

70   Pulliainen et al., 2001; Thiemann and Kaufmann, 2000; Wang et al., 2008). In addition,

71   SD, which is one of the most commonly measured trophic state indicators, has also

72   been used to assess water trophic states (Binding et al., 2015; Knight and Voth, 2012;

73   Lillesand et al., 1983; Olmanson et al., 2008; Papoutsa et al., 2014; Sheela et al., 2011b).

74   Other studies based on RS have used multiple variables to assess water trophic states

75   (Cheng and Lei, 2001; Sass et al., 2007; Xiang et al., 2015). However, most of the RS-

76   based retrieval methods make assumptions about the biogeo-optical properties of the

77   target aquatic system and have spatial-temporal limitations or high demands on the

78   spectral resolution of RS data, due to the complex optical properties of inland waters

79   (Shen et al., 2014; Spyrakos et al., 2018; Ylöstalo et al., 2014). An additional challenge

80   is the calculation of water-leaving reflectance ($R_{rs}(\lambda)$) data globally by removing

81   various and complex atmospheric effects (Chen et al., 2013a; Wang et al., 2016),

82   although several atmospheric correction models have been developed to overcome the

83   atmospheric correction problems for different types of inland waters (Hu et al., 2000;

84   Shanmugam and Ahn, 2007; Wang and Shi, 2007; Wang et al., 2011; Zhang et al., 2014).

85   Given these challenges, the development of a globally valid Earth observation approach

86   for water trophic state assessment has been hindered (Palmer et al., 2015).

87   Here, we promote a water colour index, Forel-Ule index (FUI), as the water quality

88   parameter to assess trophic state of inland waters. We chose the FUI, which divides

89   natural waters into 21 colour classes from dark blue to yellowish brown based on the

90   traditional Forel-Ule scale due to its wide covering of water optical characteristics and

91   intimate relations with water quality (Wernand and Van der Woerd, 2010; Van der

92   Woerd et al., 2016). Indeed, water colour expressed through a single colour index is

93   generally not sufficient to retrieve variables such as Chl-a or suspended sediments

94   unambiguously (Bukata, 1983; Bukata 1995). However, studies have demonstrated that

95   water colour is closely associated with the absorption and scattering effects of water

96   constituents (including Chl-a and suspended sediments), and therefore can be used to

97   reflect the comprehensive water quality (Garaba et al., 2014; Wang et al., 2015;

98   Wernand et al., 2013a). Since the FUI can be objectively retrieved using RS

99   observations at the global scale (Li et al., 2016; Wernand et al., 2013b), it could provide

100   a feasible solution to monitoring global inland water bodies.

101   The main aim of this study was to develop an FUI-based trophic state assessment

102   approach for global inland waters using the Moderate-resolution Imaging

103   Spectroradiometer (MODIS) data, and to provide a global-scale view of the water

104   quality of large lakes and reservoirs worldwide.

105   **2. Datasets**

106   **2.1 MODIS surface reflectance product**

107   The MODIS level-3 surface reflectance product (MOD09A1) provides data of

108   mapped surface spectral reflectance at 500 m spatial resolution from 7 bands across the

109   visible and near infrared and short-wave infrared wavelengths (i.e. 469 , 555, 645, 859,

110   1240, 1640, and 2130 nm) (Vermote and Vermeulen, 1999). MOD09A1 is an 8-day

111   composite MODIS Terra product, which is spatially divided by uniform MODIS tiles

112   on the global scale, which makes it easy to calculate global time-series statistics. It has

113   been used for long-term and large-area water quality monitoring research as this dataset

114   is well georeferenced, synthesized, and cloud marked (Hou et al., 2017; Klein et al.,

115   2017; Li et al., 2016; Wu et al., 2013).

116   In order to retrieve the FUI of global inland waters, we used more than 6400

117   MOD09A1 images taken during the summer months of 2012 acquired from the

118   Goddard Space Flight Center (GSFC) of the National Aeronautics and Space

119   Administration (NASA) (http://ladsweb.nascom.nasa.gov/index.html). We chose the

120   year 2012 because of the availability of validation data from published studies and

121   online databases about the trophic state of inland waters. Summer months (i.e. from

122   June to September in the Northern Hemisphere, and from December to March in the

123   Southern Hemisphere) were used to retrieve the FUI, because the biomass of Chl-a-

124   containing planktonic algae generally peaks in this season (Singh and Singh, 2015) and

125   therefore has the greatest effect on water colour.

126   **2.2 In-situ dataset**

127   Details of the field measured Chl-a and in-situ $R_{rs}(\lambda)$ are given in in Table 1. The

128   in-situ dataset contains 469 samplings from 10 lakes in Asia, North America, and

129   Europe. The selection represents different types of inland waters, ranging from a few

130   oligotrophic and mesotrophic lakes to more eutrophic lakes, from lakes with high total

131   suspended matter (TSM, i.e. Taihu Lake) to lakes with high coloured dissolved organic

132   matter (CDOM, i.e. Lake Peipsi and Lake Winnipeg).

133   Table1 Lake Names, locations, number of samplings (N), mean Chl-a concentrations (Chl-a, μg/L)
134   and data sources of the 10 lakes and reservoirs with field measurements

Lake	Latitude	Longitude	Chl-a	N	Data Source
Lake Maggiore	46.01 N	8.67 E	2.41	3	In-situ (Giardino et al., 2013)
Lake Winnipeg	51.9 N	97.3 W	5.33	58	In-situ (Binding et al., 2013)
Lake Erie	41.9 N	82.1 W	9.34	24	In-situ (Binding et al., 2013)
Lake Peipsi	58.47 N	27.34 E	17.95	26	In-situ (Kutser et al. 2013)
Lake Erhai	25.86 N	100.15 E	19.11	21	In-situ
Yuqiao Reservoir	40.04 N	117.55 E	20.73	13	In-situ
Guanting Reservoir	40.35 N	115.73 E	26.8	31	In-situ
Taihu Lake	31.20 N	120.18 E	42.6	239	In-situ
Chaohu Lake	31.55 N	117.57 E	64.47	29	In-situ
Dianchi Lake	24.82 N	102.71 E	85.2	25	In-situ

135   Equation (1), suggested by Carlson (1977), was applied to the Chl-a dataset:

7

$$\text{TSI(Chl-a)} = 10(6 - \frac{2.04 - 0.68 \ln Chl\text{-}a}{ln2})\hspace{2cm}(1)$$

where Chl-a denotes the concentration of Chl-a in μg/L. The TSI method classifies the water trophic state as oligotrophic (TSI < 30), mesotrophic (30 ≤ TSI < 50), or eutrophic (TSI ≥ 50). The in-situ measured $R_{rs}(\lambda)$ was used to simulate MODIS bands by using MODIS spectral response functions (SRF), and then the FUI for these samplings was calculated to determine the relationship between TSI and FUI.

Concurrent MOD09 images were acquired to build the data pairs of $R_{rs}(\lambda)$. The FUI was calculated from the data pairs and compared to evaluate the accuracy of MODIS FUI. The data pairs were coincident within a ±3 hour window and the nearest MODIS image pixel was used to pair with the in-situ data. After removing concurrent MODIS data with cloud cover, noise cover, and near shoreline pixels, there were 135 pairs of $R_{rs}(\lambda)$ data from 7 of the 10 lakes. There were 73 pairs for Taihu Lake with 13 concurrent images in July and October 2006, and January and April 2007 (Wang et al., 2016); 10 pairs for Qinghai Lake with 1 concurrent image in August 2014 (Li et al., 2016); 10 pairs for Lake Erhai with 1 concurrent image in July 2012; 17 pairs for Lake Erie (Binding et al., 2013) with 3 concurrent images in August 2012; 20 pairs for Lake Winnipeg (Binding et al., 2013) with 8 concurrent images in July and August 2012; 4 pairs for Lake Peipsi (Kutser et al., 2013) with 1 concurrent image in June 2012; and 1 pair for Lake Maggiore (Giardino et al., 2013) with 1 concurrent image in July 2012.

2.3 Hydrolight simulated dataset

156   A Hydrolight simulated Chl-a and $R_{rs}(\lambda)$ dataset published by (IOCCG, 2006) was

157   also used to improve the representativeness of oligotrophic to mesotrophic waters in

158   our dataset, and to illustrate the theoretical relationship between FUI and TSI in these

159   relatively clear waters. This dataset was simulated using the widely accepted

160   Hydrolight code (Mobley, 1995), with input inherent optical properties (IOPs)

161   generated from a wide range of field measurements with various bio-optical models not

162   limited to Case I water (IOCCG, 2006). The concentration of Chl-a in the simulated

163   dataset ranges from 0.03 to 30.0 μg/L with an average value of 6.08 μg/L.

164   **2.4 Independent validation dataset**

165   The FUI-based water trophic state assessment results for the summer of 2012 were

166   validated through comparison with published studies and online databases, including

167   China Environmental State Bulletin from Ministry of Environmental Protection of the

168   People's Republic of China (MEPPRC, 2012), and the National Lake Assessment from

169   the US Environmental Protection Agency (USEPA, 2016). To guarantee objectiveness

170   and fairness in the validation process, comparison data were only selected where they

171   represented the whole water body, and where the acquisition time was as close as

172   possible to the year of 2012. In total, 100 inland water bodies distributed around the

173   globe were used for validation (Figure 1).
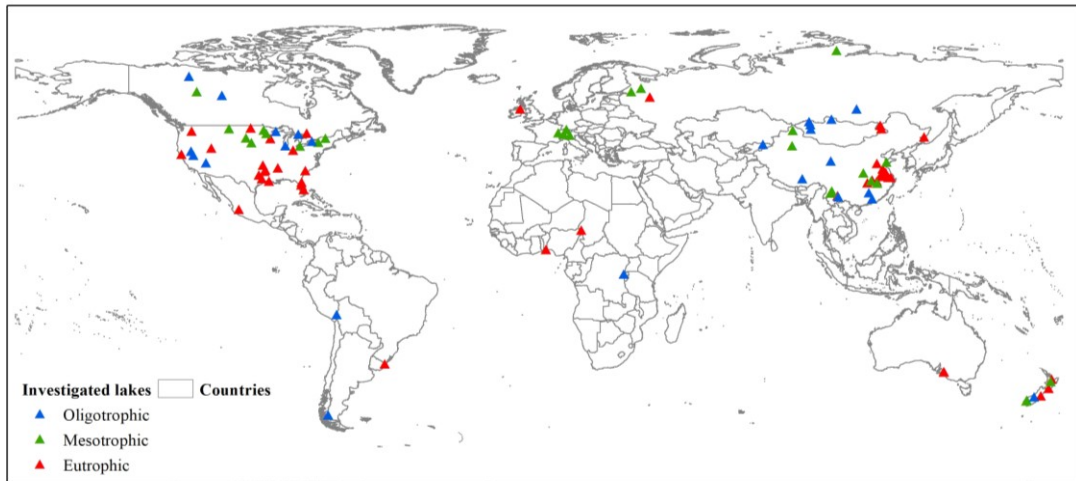
Figure 1 Spatial distribution and trophic states of 100 water bodies used for validation of the Moderate Resolution Imaging Spectroradiometer (MODIS)-derived Forel-Ule index (FUI) method. Trophic state data were obtained through literature review. Blue triangles denote oligotrophic water bodies, green triangles denote mesotrophic water bodies, and red triangles denote eutrophic water bodies.

3. Methods

3.1 Water-leaving reflectance correction

The MODIS surface reflectance products (MOD09) have been corrected for the effects of atmospheric gases, aerosols, thin cirrus clouds and adjacency from MODIS L1B data (Vermote and Vermeulen, 1999). It was found that the MOD09 reflectance was overall greater than the in situ reflectance over inland waters due to the residual noises, including the residual aerosol effect, skylight reflection, and possible sun glint (Wang, 2016). It is considered that MOD09 often fails to correct for aerosol effect because its aerosol input (the MODIS aerosol product, MOD04) usually uses a small fill value for the aerosol optical thickness for most inland waters (Wang et al., 2016; Vermote and Vermeulen, 1999). In this study, a band subtraction method based on near-

191   infrared (NIR) to short wave infrared (SWIR) bands was used to reduce the noises in

192   MOD09 data and to convert it to water-leaving reflectance ($R_{rs}(\lambda)$) (Wang, 2016). The

193   correction equation is:

194
$$R_{rs}(\lambda) = \frac{R(\lambda) - \min(R_{NIR} : R_{SWIR})}{\pi}$$
(2)

195   where $R(\lambda)$ is the original reflectance of the MOD09 band, and $\min(R_{NIR} : R_{SWIR})$ is the

196   minimum positive value of the NIR and SWIR bands. The $\min(R_{NIR} : R_{SWIR})$ was

197   subtracted from each pixel for each band to account for the residual errors (Wang and

198   Shi, 2007; Wang, 2016). This method neglects the aerosol types, but it can also avoid

199   the uncertainties in the NIR and SWIR bands being amplified by aerosol exponential

200   models. The formula is divided by π to convert the surface reflectance to water-leaving

201   reflectance by neglecting the bidirectional effects. Despite imperfections and

202   limitations, this method has been shown to achieve accuracies around 30%, and it can

203   be easily implemented in operational data processing systems for deriving $R_{rs}(\lambda)$ with

204   relative stable performances over inland waters under various conditions (Wang et al.,

205   2016).

206   **3.2 Water body identification**

207   The water bodies studied were large lakes and reservoirs (i.e., > 25 km^2 and

208   covering > 100 pixels in a MOD09A1 image). Water body extraction was taken directly

209   from satellite data rather than using a static geographic database due to the dynamic

210   nature of margins of some water bodies. The detection of water pixels in the MOD09A1

211   product was carried out using a series of processing steps on the MODIS satellite data

212   outlined in Figure 2.
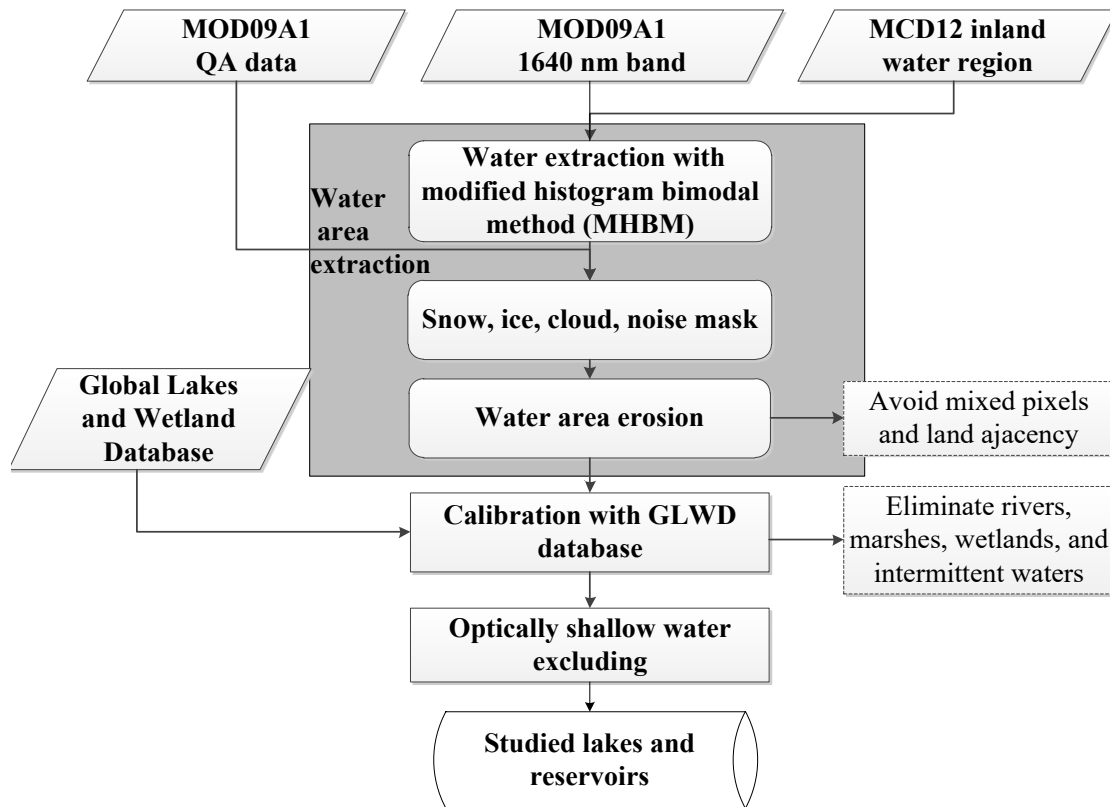
213

214   Figure 2 Flowchart of water body extraction and calibration from MOD09A1 products. MOD09A1
215   QA data is the Quality Assurance dataset that included in MOD09A1 dataset. MHBM is the
216   modified histogram bimodal method suggested by Zhang et al. (2018).

217   *3.2.1 Water body extraction and identification*

218   The modified histogram bimodal method (MHBM) suggested by Zhang et al.

219   (2018) was used to automatically segment water areas from land in the MOD09A1

220   image by using the 6th band (1640 nm) with a dynamic threshold for each water body.

221   The 1640 nm band was selected because it was strongly absorbed by water and strongly

222   reflected by terrestrial regions (Mishra and Prasad, 2015). There are six steps in the

223   segmentation process as follows:

12

224 (1) For each water body, the initial water area provided by the MODIS Land Cover

225   Type product (MCD12Q1 Type-1) (Friedl et al., 2010), which is gridded identically

226   to MOD09A1, was extended around the coastline reaching a number of 250%

227   pixels of the water area (including the initial water area).

228 (2) For each water body, a reflectance histogram of the 1640 nm band of the dilated

229   region was calculated, and the valley value of the histogram falling in the threshold

230   range was automatically determined as the threshold for the specific water body.

231   The range of thresholds from a range of representative water types was 0.005 to

232   0.11;

233 (3) Water bodies were segmented from MOD09A1 images using the determined

234   thresholds;

235 (4) MOD09A1 Quality Assurance (QA) data (Vermote et al., 2015) were used to

236   eliminate cloud, ice, and snow cover, and low quality pixels from the water areas;

237 (5) Extracted water areas were eroded with a 500 m buffer to avoid the effects of mixed

238   land-water pixels and severe land adjacency near the shoreline and to ensure the

239   quality of water pixels (Hou et al., 2017);

240 (6) Water bodies with areas of water connected with more than 100 pixels (i.e., > 25

241   km^2) were selected for this study.

242   The 500 m buffer was determined according to the comparison of MODIS $R_{rs}(\lambda)$

243 in the transects selected from the land–water boundaries; it showed that generally, one

244 pixel (500 m) near the shoreline at the visible bands was subject to detectable adjacency

245 contamination, which is consistent with the findings of Hou et al. (2017). Notably, the

246 land adjacency effect for MODIS may theoretically have an impact at much larger

247 distances offshore (Bulgarelli and Zibordi, 2018), but considering that the uncertainty

248 in MODIS $R_{rs}(\lambda)$ is already approximately 30%, the adjacency effect at distances greater

249 than 500 m may not be obvious.

250   Figure 3 shows the examples of water segmentation from MOD09A1 data. It

251 demonstrates that the water pixels have characteristically low reflectance values which

252 aids in detection against different land cover types, including small islands (Figure 3 (b)

253 and (c)), clouds (Figure 3 (f) and (g)), snow and ice (Figure 3 (e)), aquatic plants (Figure

254 3 (g)) and low quality pixels (Figure 3 (g)). The $R_{rs}(1640)$ values of the intersect lines

255 (marked in Figure 3) under different conditions are shown in Figure 4.

256   The extracted water areas were intersected with the Global Lakes and Wetland

257 Database (GLWD) (Lehner and Döll, 2004), which represents a compilation of

258 numerous existing maps and datasets and has been validated comprehensively for lakes >

259 1 km^2. GLWD Level 3 (GLWD-3) comprises lakes, reservoirs, rivers and different

260 wetland types in the form of a global raster map at 30-second resolution. Since the aim

261 of this study is to assess the trophic state of lakes and reservoirs at the global scale,

262 water bodies with centroid points located in the lake or reservoir type in the GLWD-3

263 database were chosen, and those located in rivers, ephemeral waters, coastal wetland

264   and other types of wetland were removed.
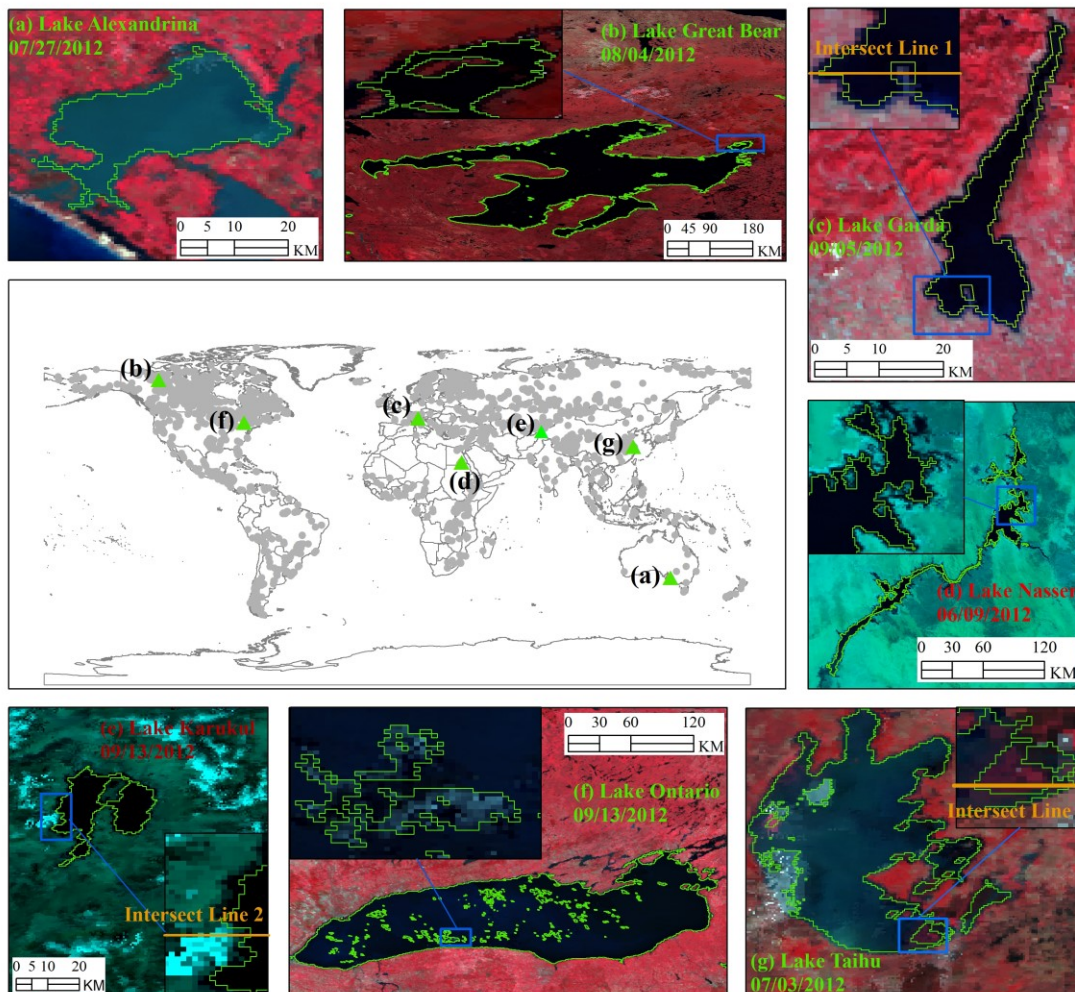
266   Figure 3 Shorelines of water bodies extracted from MOD09A1 images using the modified histogram
267   bimodal method (MHBM). (a) Lake Alexandrina in Australia; (b) Lake Great Bear in North America;
268   (c) Lake Garda in Europe; (d) Lake Nasser in Africa; (e) Lake Karukul in Asia; (f) Lake Ontario in
269   North America; (g) Lake Taihu in Asia. Green lines denote shorelines. Backgrounds are standard
270   false colour images where red, green, and blue are the 859 nm, 645 nm and 555 nm bands of the
271   MOD09A1 image, respectively. The image acquisition date is listed in each subfigure. The $R_{rs}(1640)$
272   values of the three intersect lines are shown in Figure 4.
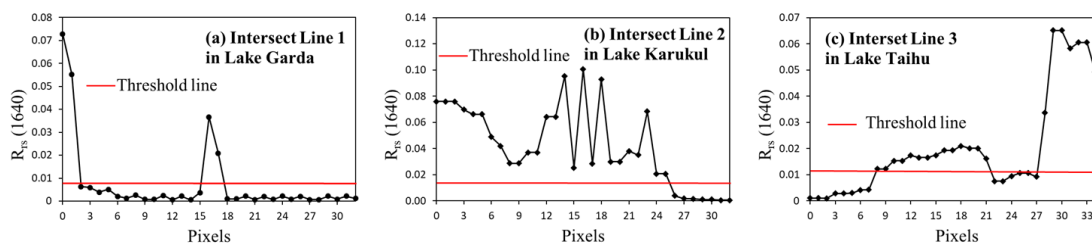
274   Figure 4 The $R_{rs}(1640)$ values of the intersect lines that marked in Figure 3. (a) Intersect Line 1

275 through Lake Garda crosses an island inside the lake; (b) Intersect Line 2 through Lake Karukul
276 crosses snow covering the shore side; (c) Intersect Line 3 through Lake Taihu crosses obvious
277 aquatic plants in the water.

278 *3.2.2 Excluding optically shallow water*

279   The extracted water pixels were tested for optically shallow water. Even though

280 optically shallow water for large inland waters (>25 km^2) is seldom found once the

281 identified wetlands in GLWD database are removed, it is possible that bottom

282 reflectance may influence observed water colour, for example in arid or semi-arid saline

283 lakes. Numerous radiative transfer models have been developed that account for the

284 effects of the bottom reflectance and water column on remotely sensed $R_{rs}(\lambda)$ (Lyzenga,

285 1978; Philpot, 1989; Maritorena et al., 1994; Lee et al., 1998; Mobley and Sundman,

286 2003). The response types of $R_{rs}(\lambda)$ spectral curves differ with changes in bottom status,

287 water depth, and optical properties of the water (Holden and LeDrew, 2002; Ma et al.,

288 2014; Lee et al., 1998；Lim et al., 2009), and there is no single method that can

289 accurately detect optically shallow water in lakes at the global scale.

290   To address these challenges, a three-stage method combining automatic

291 identification with manual-intervention was used to identify the optically shallow water

292 bodies:

293 (1) The MODIS SWIR band (1640 nm) threshold method was adopted in water area

294   segmentation, so that shallow waters with benthic aquatic plants were eliminated

295   from water area due to the higher reflectance in the SWIR band from the aquatic

296   plant that would not be presented in deeper waters (Li et al., 2009);

16

297   (2) The blue band threshold method was used as a preliminary means for identifying

298   shallow waters containing a signal from highly reflective sand and sediment

299   bottoms (Lim et al., 2009; Mobley and Sundman, 2003). The threshold (R_{rs}(469

300   nm) = 0.015 sr^{-1}) was determined by collecting and comparing a large number of

301         $R_{rs}(\lambda)$ spectra of optically shallow and deep waters derived from MOD09A1

302   images in the summer of 2012 (Figure 5);

303   (3) Shallow water bodies identified in the first two steps were reviewed using Google

304   Earth and relevant publications (Williams, 2002; Hurlbert, 2012), to remove lakes

305   and reservoirs characterized by deep waters.
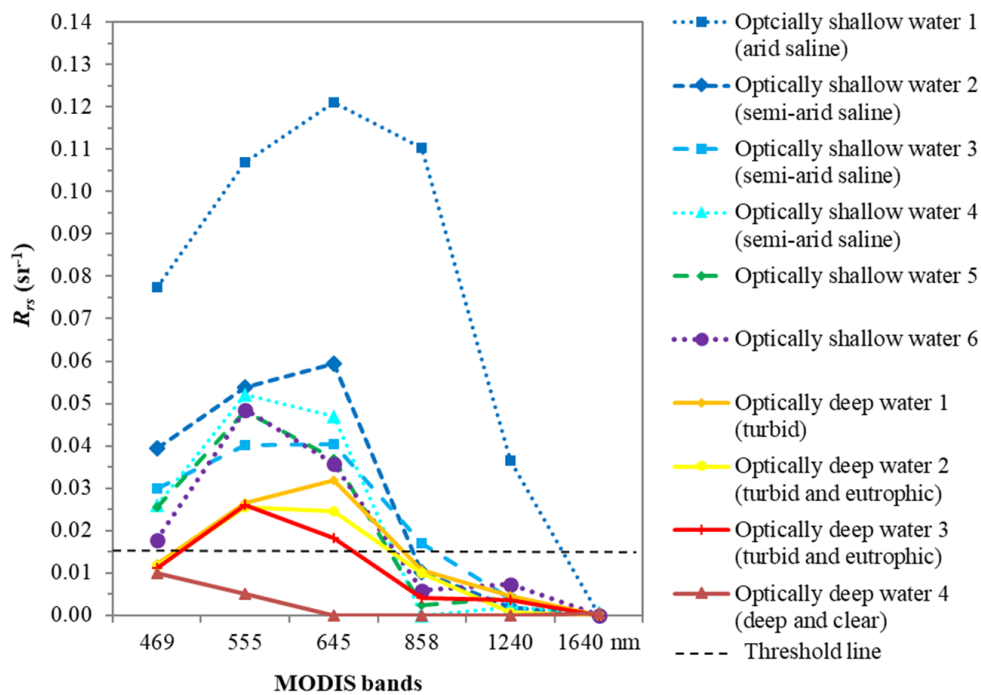
306
307   Figure 5 Typical water-leaving reflectance ($R_{rs}(\lambda)$) spectra of optically shallow waters and optically
308   deep waters derived from MOD09A1 images in the summer of 2012. The optically shallow waters
309   1-4 are Lake Beihuo Luxun, Lake Manas, Lake Margai Caka, and Lake Gasi Kule from Northwest
310   China, and they were described as arid and semi-arid saline lakes in Wang and Dou (1998). The
311   identified optically shallow waters 5 and 6 are Lake George in Australia (Fitzsimmons and Barrows,
312   2010) and shallow water near the island bank in the Bahamas, respectively (Dierssen et al., 2003);

17

313 The dotted line denotes the threshold line (0.015 sr^{-1}) of R_{rs}(469 nm) that used to separate the

314 optically shallow waters.

3.3 FUI retrieval method

316 In the Commission on Illumination (CIE) colourimetry system, theoretically colour

317 parameters can be calculated from hyperspectral $R_{rs}(\lambda)$ and colour-match functions by

318 using spectral integration in the visible range (C.I.E., 1932; Wang et al., 2015). As there

319 are only three red, green, blue (RGB) bands in MOD09 images (645 nm, 555 nm and

320 469 nm), the RGB conversion method was used to calculate CIE X, Y, Z using the $R_{rs}(\lambda)$

321 at the three visible bands (Wang et al., 2015; Li et al., 2016). The RGB conversion

322 equation to X, Y, Z is as follows:

323
$$X = 2.7689R + 1,7517G + 1.1302B$$

324
$$Y = 1.0000R + 4.5707G + 0.0601B$$

325
$$Z = 0.0000R + 0.0565G + 5.5934B \tag{3}$$

326 CIE chromaticity coordinates (x, y) were then calculated from the X, Y, Z by

327 normalizing them to between 0 and 1. A new coordinate system (x', y') was built based

328 on the chromaticity coordinates (x, y) as (Figure 6):

329
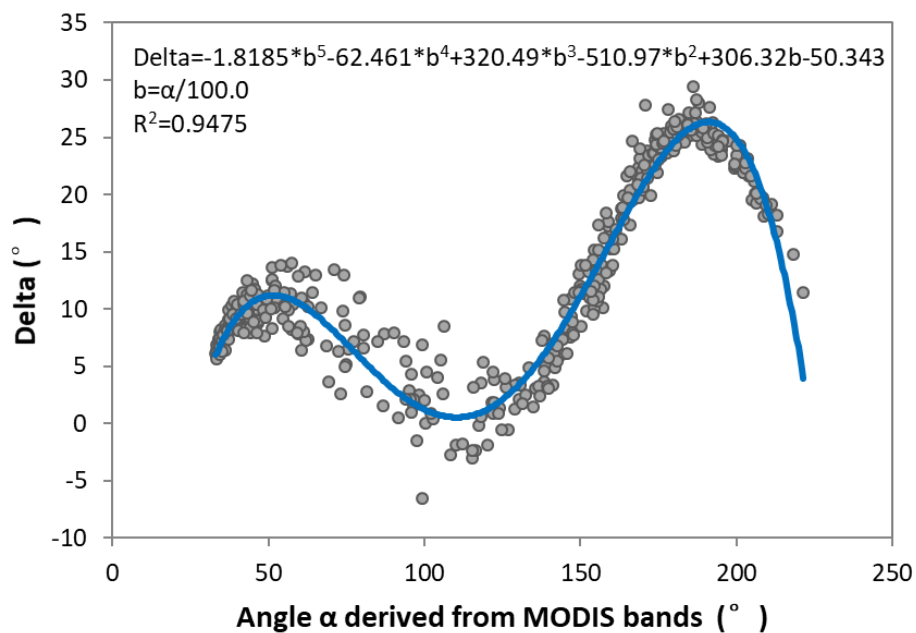$$x' = y - \frac{1}{3}$$

331
$$y' = x - \frac{1}{3}$$

330
$$\tag{4}$$

332 Based on the coordinates (x', y') in the CIE chromaticity diagram, angle α was

333 calculated, defined as the angle between the vector of coordinates (x', y') and the

18

334 negative x'-axis (at y = 1/3) in the new coordinate system. It is notable that angle α is

335 basically consistent with the definition reported in Wang et al. (2015); but for the

336 convenience of subsequent calculation, starting from the negative x'-axis, the angle α

337 is improved to remain positive now from 0° to 360°. Due to the band setting of satellite

338 sensors, there is a difference between the human eye sensed true colour and the sensor

339 derived colour (Van der Woerd and Wernand, 2015). To eliminate the colour difference

340 caused by MODIS band setting, a systematic deviation delta, defined as the difference

341 between angle α derived from hyperspectral $R_{rs}(\lambda)$ and the equivalent MODIS bands,

342 was modelled and calculated. Following the method presented in Van der Woerd and

343 Wernand (2015), the delta for MODIS was modelled with a polynomial fitting (Figure

344 7) based on the simulated dataset generated by Hydrolight (IOCCG, 2006). With this

345 delta correction, the angle α and the FUI can be transferable between satellites and

346 sensors with different spectral settings (Van der Woerd and Wernand, 2015). Finally,

347 based on angle α after delta correction, the FUI was calculated using the 21-class FUI

348 lookup table established from the chromaticity coordinates of the Forel-Ule scales

349 (Novoa et al., 2013, Figure 6).

350
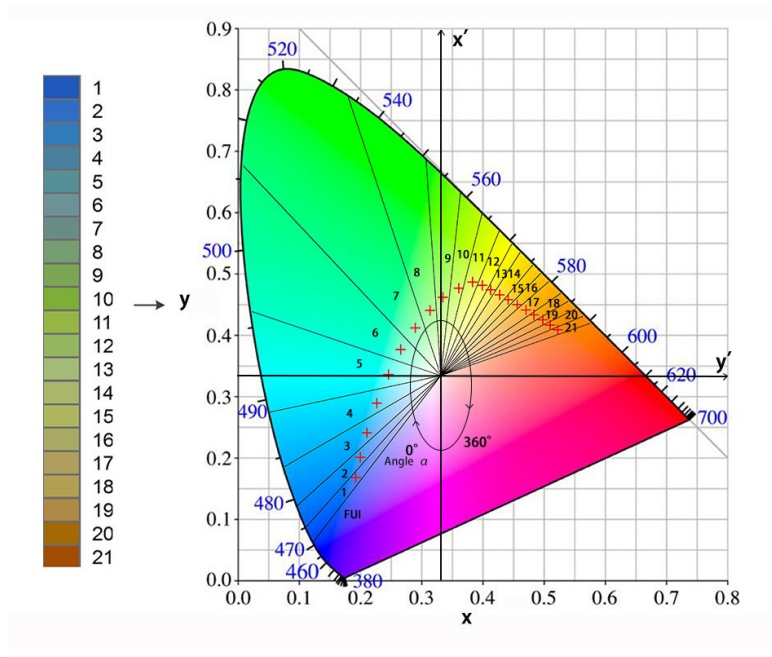
Figure 6 The FUI colours and the subdivision of the FUI from 1 to 21 in the CIE chromaticity diagram. The red crosses mark the chromaticity coordinates of the Forel-Ule scales (Novoa et al., 2013). Angle α is the angle between the vector to a point and the negative x'-axis (at y = 1/3).

Delta$=-1.8185*b^5-62.461*b^4+320.49*b^3-510.97*b^2+306.32b-50.343$
$b=\alpha/100.0$
$R^2=0.9475$

354

Figure 7 Deviation delta (°) from the hyperspectral angle α as a function of MODIS derived angle α for 0° < α < 230° (i.e., FUI ranging from 1 to 20)

### 3.4 FUI-based trophic state assessment algorithm

Calculations of the FUI and TSI were initially derived from the Hydrolight

20

359   simulated dataset to build the theoretical relationship between the two quantities in

360   relatively clear Chl-a dominated waters (Figure 8). Values for TSI ranged from 0 to 68,

361   the FUI generally increased with TSI based on the simulated dataset ($R^2 = 0.94$, N =
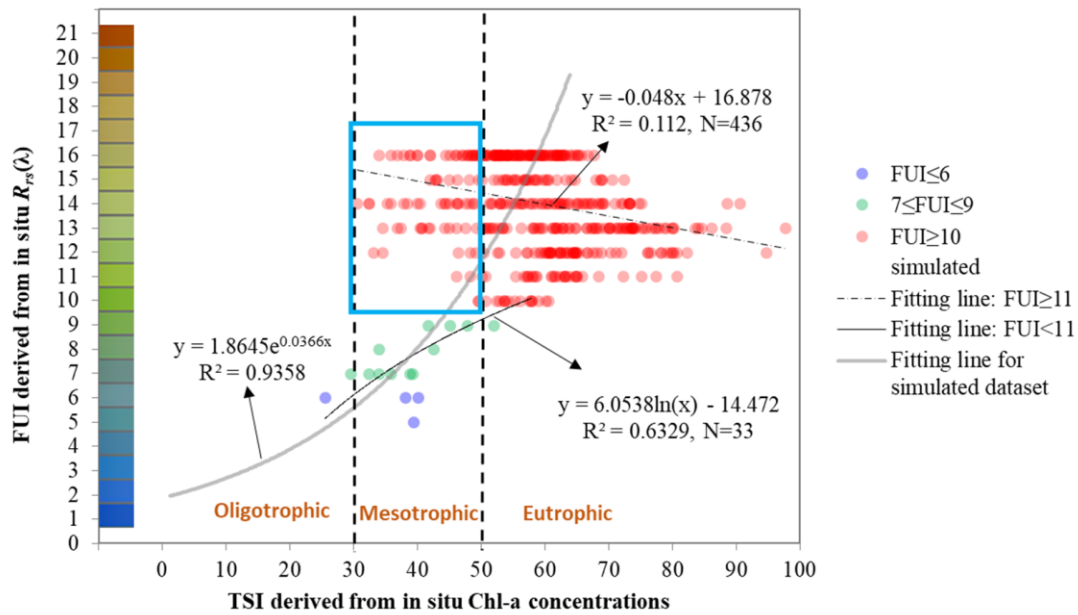
362   500).

363   However, the relationship between FUI and TSI from the in-situ dataset (Table 1)

364   showed a unimodal distribution (Figure 9): (i) similar to the simulated dataset, when

365   FUI < 10, it increased with TSI ($R^2 = 0.633$), showing that when water colour changes

366   from blue to green, the water body changes from oligotrophic to mesotrophic; (ii) TSI

367   peaked when FUI approached 10, because highly eutrophic waters generally appear

368   green owing to high Chl-a content; (iii) when FUI > 10, it showed a scattered negative

369   relationship with TSI ($R^2 = 0.112$), reflecting the shift from green to brown associated

370   with turbid eutrophic, or humic waters. Based on the in-situ dataset, the relationship for

371   FUI >10 is scattered and loose (Figure 9) because of complex constituents varying

372   independently in turbid waters, but this occasion is underrepresented in the simulated

373   dataset in Figure 8.

374   Although there are insufficient oligotrophic and mesotrophic waters in the in-situ

375   dataset, the in-situ dataset in Figure 9 showed a roughly similar overall trend as the

376   simulated dataset in Figure 8, and presented the FUI ranges for different trophic states.

377   The dataset showed that 82.7% of in-situ data points with FUI values ≥ 10 were

378   eutrophic with TSI ≥ 50; 83.3% of points with 7 ≤ FUI < 10 (i.e., 10 points out of 12)

379   were mesotrophic while the other two points had TSI values of 29.5 and 50.5. Finally,

380   data points with FUI < 7, were classified as oligotrophic, which is supported by the

381   simulated dataset. The FUI ranges were consequently used to classify the trophic state

382   of the waters.
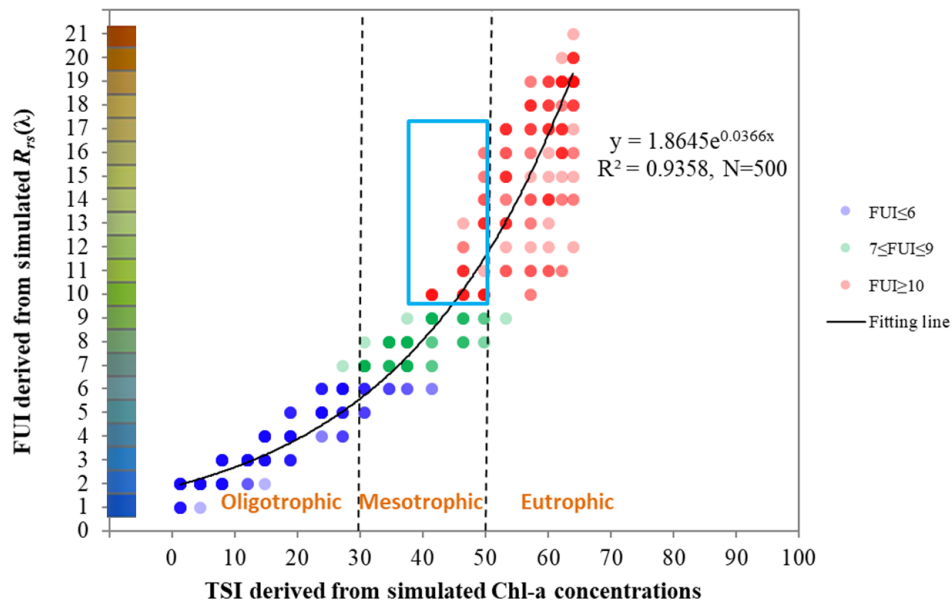
383

384   Figure 8 Scatterplot of data pairs of the Forel-Ule index (FUI) and Chl-a-based trophic state index
385   (TSI) from the Hydrolight simulated dataset (N = 500) (IOCCG, 2006). The colour bar indicates the
386   colour of the FUI indices. This simulated dataset covers a wide range of natural waters with
387   concentrations of Chl-a from 0.03 to 30.0 μg/L . The points were plotted with 60% transparency to
388   show the data density. The cyan box marks the mesotrophic points with FUI ≥ 10.

Figure 9 Scatterplot of data pairs of the Forel-Ule index (FUI) and concurrent Chl-a-based trophic state index (TSI) from in-situ measurements (N = 469). The colour bar indicates the colour of the FUI indices. Blue points denote FUI ≤ 6, green spots denote 7 ≤ FUI ≤ 9, and red spots denote FUI ≥ 10. The spots were plotted with 60% transparency to show the density of observations. The cyan box marks the mesotrophic points with FUI ≥ 10.

Some humic (i.e., high CDOM content) or turbid (i.e., high TSM content) mesotrophic waters may result in an FUI value greater than 10 with green to brown colour, such as the scattered points presented in the cyan box in Figure 8 and Figure 9. To distinguish these points, a red band (R_{rs}(645)) threshold method was implemented by comparing the $R_{rs}(\lambda)$ spectra of these points with representative $R_{rs}(\lambda)$ spectra of eutrophic waters. Even if water bodies with high CDOM but low TSM appear with a high colour index, R_{rs}(645) will be relatively low compared with other TSM-dominated yellow waters due to low backscattering of the water constituents with high CDOM and low TSM. After applying this threshold, the accuracy of eutrophic classification was increased to 86.8%. With the FUI subsection and the R_{rs}(645) threshold, a decision tree

23

405 of trophic state assessment for water bodies was developed, shown in Figure 10.

406

FUI

FUI < 7 | 7 ≤ FUI < 10 | FUI ≥ 10

$R_{rs}(645) \leq 0.00625$

Oligotrophic | Mesotrophic | Eutrophic
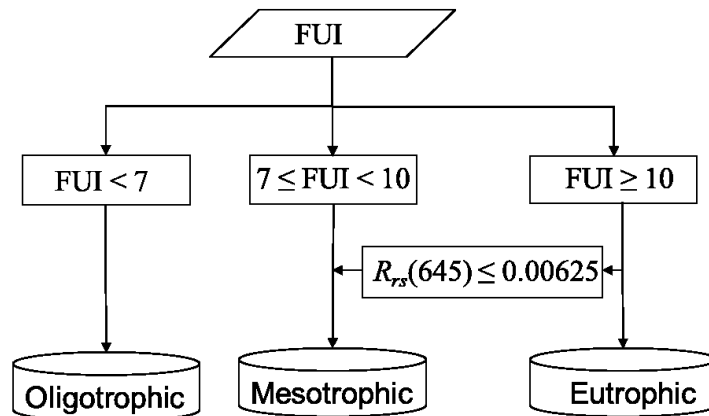
407
408 Figure 10 Forel-Ule index (FUI)-based water trophic state assessment decision tree based on the
409 classification of FUI and $R_{rs}(645)$

410   Lake-average values were considered more appropriate for global applications of

411 the method. Results showed a positive relationship between lake-average FUI and lake-

412 average TSI. For the 10 lakes sampled during 14 field campaigns, only 1 pair of

413 FUI/TSI averages was misclassified based on the FUI from the 10-lake in-situ dataset,

414 supporting the applicability of the method to lake averages.

415 **3.5 Spatial and Temporal statistics**

416   As MOD09A1 is an 8-day composite product, there are globally 16 periods of

417 MOD09A1 images over the four summer months. The seasonal average FUI for each

418 study lake was estimated and used to assess the trophic state of lakes in the summer of

419 2012. During the calculation, a standard water mask image was produced for each lake

420 by overlaying the water mask images in the same MODIS tile. This was used to check

421 the percentage of noise pixels covered by clouds, ice, snow, and other noises. If the

422 detected water pixels for a lake in an image was less than 30% of its standard water

423   mask area, then those pixels were not considered to represent the entire lake and the

424   image was not used for lake assessment. If less than 3 of the 16 images were valid for

425   a lake over the summer months, then the lake was not assessed in this study. A water

426   body spanning more than one tile of the MOD09A1 image was merged into a single

427   lake by detecting the connected area in the standard water mask images across tiles. To

428   show the variations within each lake, the spatial coefficient of variation (CV = δ/μ,

429   where δ is the standard deviation and μ is the mean) of the FUI and the temporal

430   coefficient of variation for each study lake was also calculated. The average $R_{rs}(645)$

431   for each lake was computed to aid the FUI-based trophic state assessment.

432   **4. Results**

433   **4.1 Evaluation of MODIS retrieved FUI**

434   The FUI values derived from MOD09 $R_{rs}(\lambda)$ and concurrent in-situ $R_{rs}(\lambda)$ were

435   compared to evaluate the FUI retrieved from MODIS with the water-leaving reflectance

436   correction. Despite a few scattered points (with light red colour in Figure 11(a)) that

437   may be caused by the complex atmospheric conditions (e.g. land aerosols), the paired

438   data from the seven lakes showed a strong correlation that mostly fell along the

439   approximate 1:1 line (Figure 11; R^2 = 0.87, slope = 0.92), with a mean absolute

440   difference (MAD) of 0.85 and a mean relative difference (MRD) of 7.5%. In addition,

441   the MODIS FUI produced a 10.5% difference in trophic state classification, compared

442   with the FUI derived from in-situ $R_{rs}(\lambda)$. The effects of various aerosol and

443   solar/viewing geometry perturbations on the FUI calculation are discussed in Section

444   5.1.
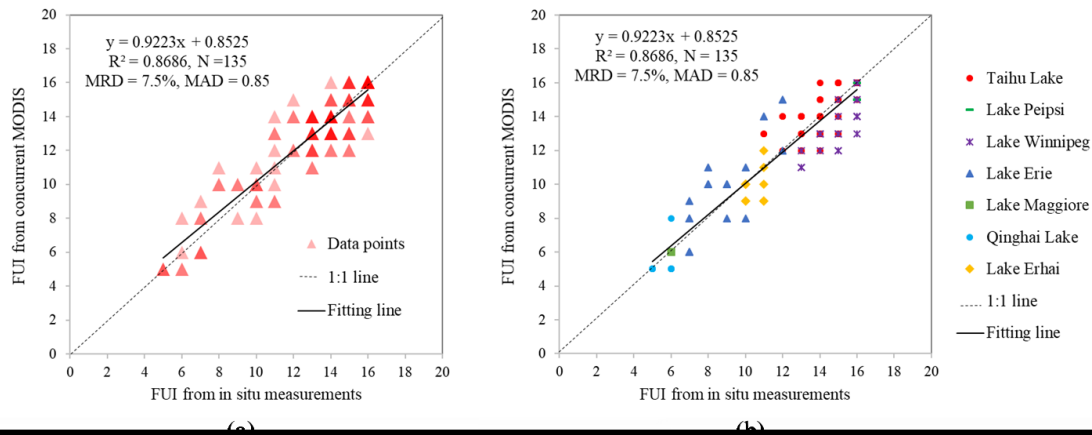
445

446 Figure 11 Scatterplots of the FUI derived from in-situ measured $R_{rs}(\lambda)$ versus concurrent MOD09
447 retrieved $R_{rs}(\lambda)$ for seven lakes with different FUI ranges. (a) Data points are coloured with 60%
448 transparency; darker spots indicate a higher data density. (b) Data points from different lakes are
449 marked with different symbols.

4.2 Validation results with independent data

451   The lake trophic state data included in the independent validation dataset, as well

452 as the sources of the trophic states data, are listed in Table S1 in Supplementary Material.

453 We found that 20 of the 100 water bodies were misclassified using the FUI-based

454 method. There were no misclassifications between eutrophic and oligotrophic water

455 bodies. Most misclassifications occurred between eutrophic and mesotrophic water

456 bodies, and to a lesser extent between mesotrophic and oligotrophic water bodies. The

457 user accuracy of the oligotrophic, mesotrophic, and eutrophic classifications was

458 100.0%, 66.7%, and 78.3%, respectively, calculated through confusion matrix analysis.

459 The overall accuracy of the trophic state assessment was found to be 80.0% ($R^2 = 0.75$),

460 while the Kappa coefficient (Landis and Koch, 1977) was 0.67 (Table 2), which

461   confirmed that the FUI-based results were substantially consistent with the comparison

462   dataset.

463   Table 2 Confusion matrix of Forel-Ule index (FUI)-based trophic state assessment for the
464   investigated 100 lakes

| Comparison Data / FUI-based Assessment	Oligotrophic	Mesotrophic	Eutrophic	Total	User accuracy
Oligotrophic	19	0	0	19	100.0%
Mesotrophic	5	14	2	21	66.7%
Eutrophic	0	13	47	63	78.3%
Total	24	27	49	100	
Producer accuracy	79.2%	51.9%	95.5%		
Kappa coefficient	0.67				
Overall accuracy	80.0%				

465

4.3 Trophic state assessment for global inland waters in 2012

467   Among the water bodies studied (N = 2058, total surface area = 1.73 million km^2),

468   the MODIS FUI of the lakes in the summer of 2012 ranged from 2.0 to 17.0, the spatial

469   CV of the water bodies ranged from 0.0% to 41.2% with an average value of 12.9%

470   and the temporal CV ranged from 0.0% to 54.3% with an average value of 9.9%. The

471   season-averaged FUI values of the studied large lakes were found to vary between 3.1

472   and 16.0, and the mean FUI was 11.1 with a worldwide CV of 26.6% (Figure 12). Based

473   on these data, the results presented that large lake trophic states were not equally

474   distributed around the globe, shown in Figure 13. Eutrophic water bodies accounted for

475   63.1% of the total number but only 30.5% of the total surface area, mesotrophic water

476   bodies accounted for 26.2% of the total number and 39.4% of the total surface area, and

477   oligotrophic water bodies accounted for 10.7% of the total number but 30.1% of the

478   total surface area.
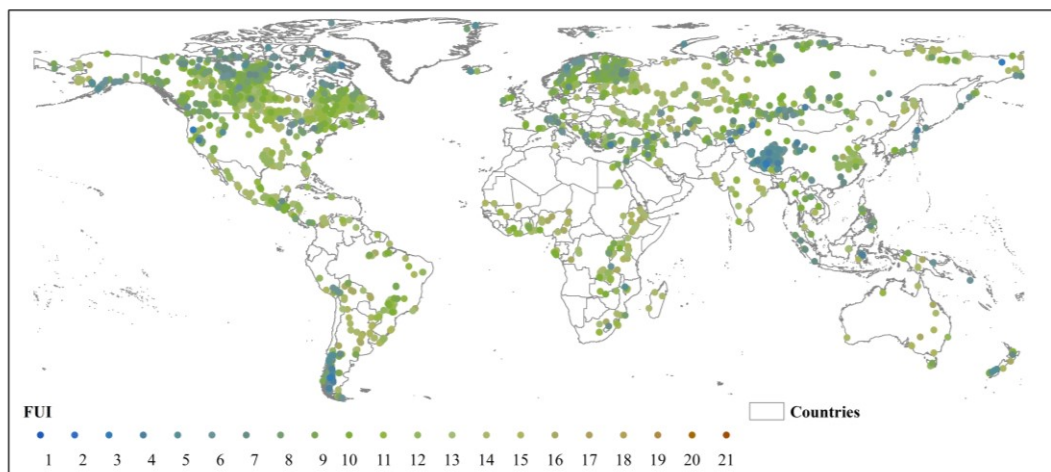
479

480   Figure 12 MODIS FUI values for global inland waters in the austral and boreal summers of 2012.
481   Each point represents a single water body of > 25 km^2 in surface area. The FUI of each point
482   represents averaged values from all lake pixels across the summer months rounded to the nearest
483   integer.
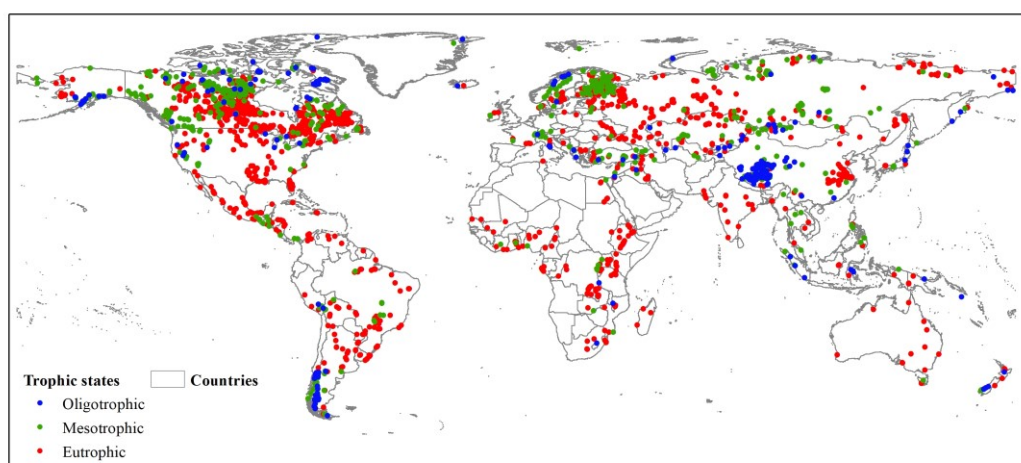
484

485   Figure 13 Trophic state classification of global inland waters in the austral and boreal summers of
486   2012 assessed using the FUI-based method. Blue spots denote oligotrophic water bodies, green spots
487   denote mesotrophic water bodies, and red spots denote eutrophic water bodies.

488   It was found that oligotrophic large lakes concentrated in high mountains and

489   plateau regions of Central Asia (Qinghai-Tibet Plateau region) and southern South

490   America (Patagonia Plateau region), while eutrophic large lakes concentrated in central

28

491   Africa, eastern Asia (East China), and mid-northern and southeast North America

492   (south Canada and southeast U.S.). In terms of lake numbers, Oceania had the highest

493   proportion of oligotrophic large lakes (23.1%), Europe had the highest proportion of

494   mesotrophic large lakes (35.2%), and Africa had the highest proportion of eutrophic

495   large lakes (88.8%). In terms of surface area, North America had the highest proportion

496   of oligotrophic water (49.8%), Asia had the highest proportion of mesotrophic water

497   (71.2%), and Africa still had the highest proportion of eutrophic water (Figure 14).
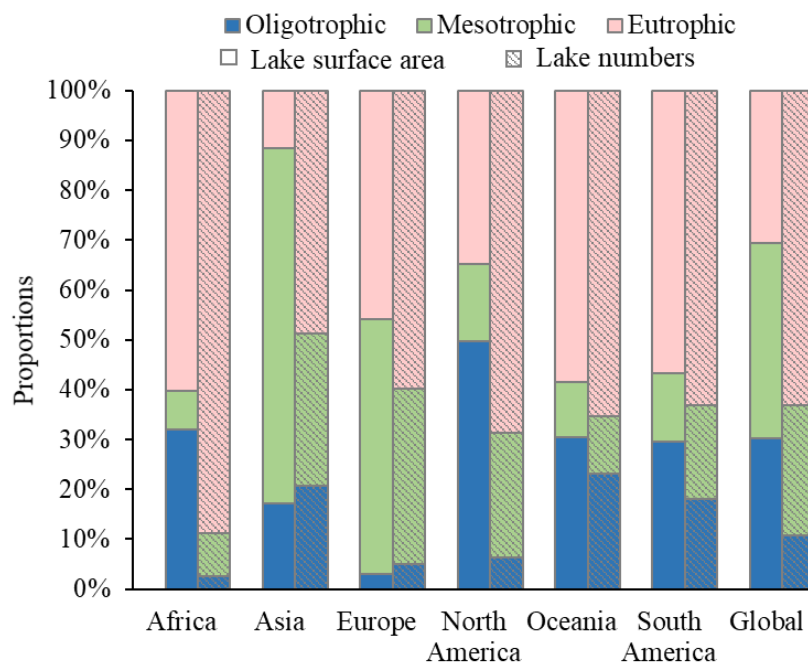
498
499 Figure 14 Proportion of large lakes with each trophic state in terms of lake number and lake
500 surface area across continents.

4.4 Trophic state assessment for regional groups of lakes

502   To further validate the FUI-based trophic state results, data from five regional

503 groups of lakes around the world were analyzed (Figure 15): the North America Great

504 Lakes region (oligo-mesotrophic dominated), the African Great Lakes region

505 (mesotrophic dominated), the central south European region (mesotrophic dominated),

506 the east Asian middle-lower Yangtze region (eutrophic dominated), and the Tibet

507 Plateau (oligotrophic dominated).
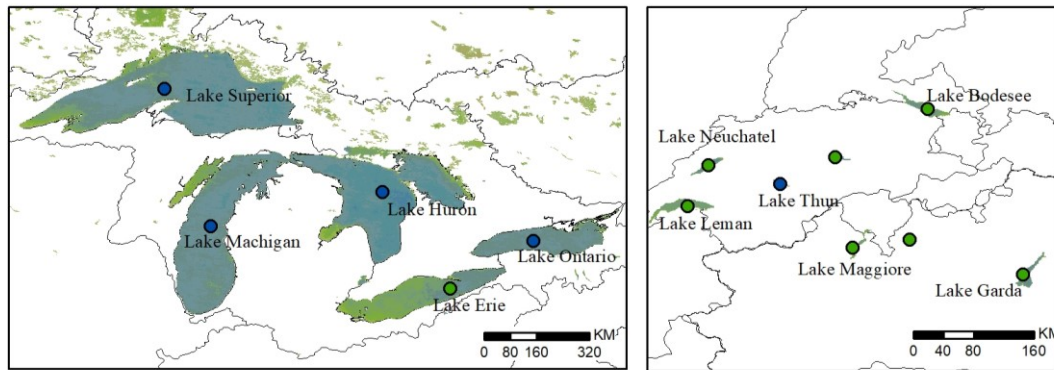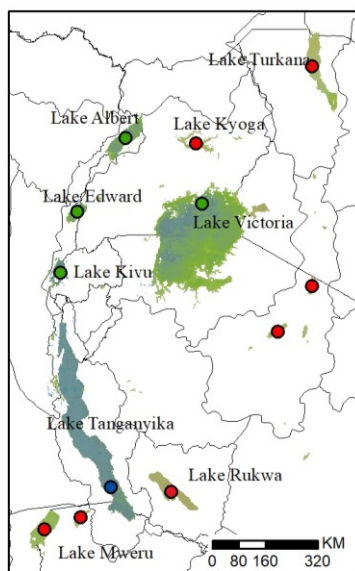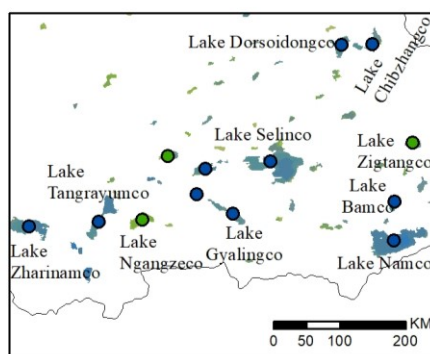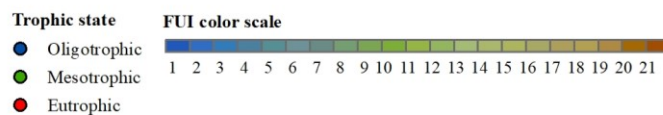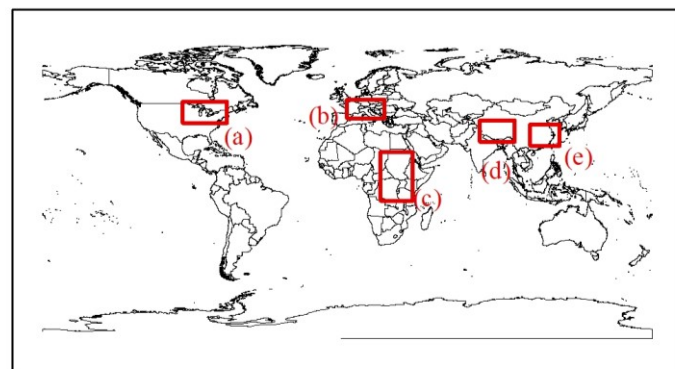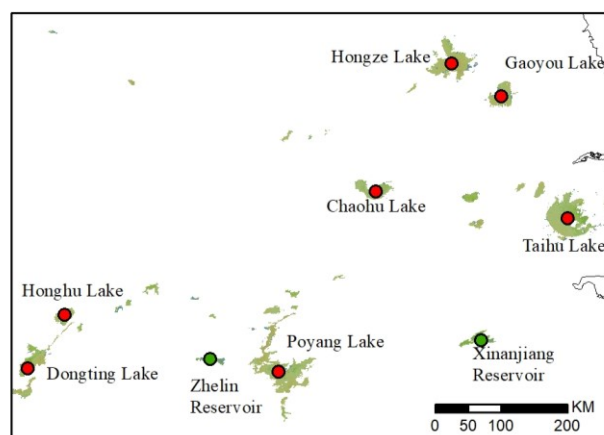
508

509　Figure 15 Trophic states and Forel-Ule index (FUI) values of large lakes within typical lake regions
510　in the austral and boreal summers of 2012: (a) North America Great Lakes region; (b) central south
511　European; (c) African Great Lakes region; (d) Tibet Plateau; (e) middle-lower Yangtze region.
512　Coloured points represent the mean trophic state of the water body (blue spots denote oligotrophic
513　water bodies, green spots denote mesotrophic water bodies, and red spots denote eutrophic water
514　bodies).

515

516　　　　The FUI of lakes in the North America Great Lakes region mainly ranged from 5

517　to 10, corresponding to a cyan water colour. Lake Superior, Lake Michigan, Lake

518　Ontario and Lake Huron were found to be oligotrophic, while Lake Erie was found to

519　be mesotrophic. The water colour of western Lake Erie is greener than the other lakes

520　and had an FUI of ~11 (i.e., eutrophic). These results are consistent with those of past

521　studies (Auer et al., 2004; Barbiero et al., 2012; Bridgeman et al., 2013; Chaffin et al.,

522　2011; Holeck et al., 2015; Mukherjee et al., 2016; Shuchman, 2013).

523　　　　The FUI of lakes in the central south European region mainly ranged from 7 to 9,

524　corresponding to a cyan water colour and a mesotrophic state. This is consistent with

525　past studies, which have classified water bodies in this region as oligo-mesotrophic

526　(Coci, et al., 2015; Rimet et al., 2015; Fuentes et al., 2013; Giardino et al., 2014; Jaquet,

527　2013; Stich and Brinker, 2010; Vollenweider and Kerekes, 1982).

528　　　　The FUI of lakes in the African Great Lakes region, which constitutes part of the

529　Rift Valley and East African Rift, mainly varied from 4 to 16, corresponding to a water

530　colour of cyan to green and a wide range of trophic states (oligotrophic, mesotrophic,

531　and eutrophic). Lake Victoria, the second largest freshwater lake in the world, is

532   mesotrophic with eutrophic sections. Lake Turkana, one of the largest desert lakes in

533   the world and the most important regional source of fish, is eutrophic. Lake Tanganyika,

534   the deepest lake in Africa, is oligotrophic. These results are consistent with the past

535   studies (Hecky et al., 2010; Okullo et al., 2011; Avery, 2012; Velpuri et al., 2012;

536   O'Reilly, 2003; Verburg, 2006).

537   The FUI of lakes on the Tibet Plateau ranged from 2 to 7, corresponding to a water

538   colour of blue to cyan and trophic states that are mainly oligotrophic. Lake Namco,

539   which lies at an elevation of 4718 m and experiences low impact from human activity

540   (Wang and Dou, 1998), was shown to have a very low FUI (2–4) and be oligotrophic.

541   Compared with Lake Namco, the FUI of Lake Selinco was higher (4–7), and its trophic

542   state was oligotrophic but approaching mesotrophic (Li et al., 2016). The FUI of Lake

543   Ngangzeco and Lake Zigtangco were found to be even higher and their trophic states

544   were mesotrophic. Few studies have been implemented for the water trophic states on

545   the Tibet Plateau due to the poor weather conditions. The results in Figure 15 (d) can

546   fill the knowledge gap in this region.

547   The FUI of the lakes in the middle-lower Yangtze region mainly ranged from 9 to

548   14, corresponding to a water colour of green to yellow-green, and the trophic states

549   were mainly eutrophic. This is consistent with past studies, which have demonstrated

550   that Lake Taihu, Lake Chaohu, Lake Poyang, and Lake Dongting are typical eutrophic

551   and turbid lakes in China (Chen et al., 2013a, 2013b; Shi et al., 2015; Wang et al., 2011;

552　Wu et al., 2013; Yang et al., 2013). The trophic states of the Xin'anjiang and Zhelin

553　reservoirs, the two largest reservoirs on the middle-lower reach of the Yangtze, were

554　found to be mesotrophic, which agrees with the results of published literature (Chen,

555　2009; Sheng et al., 2015).

5. Discussion

556

5.1 FUI sensitivity to aerosol perturbations and observation conditions

557

558　　　The significant positive correlation between the concurrent FUIs over a wide range

559　of lakes, and the relatively low uncertainties suggest that MODIS surface reflectance

560　data and the water-leaving correction method can be used for FUI retrieval and the FUI-

561　based trophic state assessment of water bodies. Moreover, it is notable that in

562　comparison with concurrent in-situ data (Figure 11), the accuracy of the MODIS FUI

563　(~90%) was greater than that of MODIS $R_{rs}(\lambda)$ (Wang et al., 2016), indicating that the

564　FUI calculation process can reduce uncertainties introduced in MODIS $R_{rs}(\lambda)$.

565　　　However, the MOD09 $R_{rs}(\lambda)$ retrieved still theoretically contains some of the

566　uncertainties induced by the effects of aerosol types and bidirectional properties as a

567　result of the MOD09 data and the water-leaving correction method. Hence, the

568　sensitivities of FUI to these uncertainties within the input data were investigated using

569　radiative transfer model simulations. These simulations verified the general global

570　applicability of FUI calculated with this method.

571　　　Based on the radiative transfer theory and assuming a non-coupling water-

572   atmosphere system, Rayleigh-corrected reflectance (R_{rc}) can be expressed as:

573 $$R_{rc}(\lambda) = \rho_t(\lambda) - \rho_r(\lambda) = \rho_a(\lambda) + \pi t(\lambda)t_0(\lambda)R_{rs}(\lambda) \qquad (5)$$

574   where $\rho_t(\lambda)$ is the top-of atmosphere (TOA) reflectance, $\rho_r(\lambda)$ is the reflectance due to

575   Rayleigh scattering, $\rho_a(\lambda)$ is the aerosol reflectance including that from aerosol

576   scattering and aerosol-Rayleigh interactions, $t(\lambda)$ is the atmospheric transmittance from

577   the target to the satellite sensor, and $t_0(\lambda)$ is the atmospheric transmittance from the Sun

578   to the target. These unknowns can be calculated from SeaDAS LUTs (look-up tables)

579   for variable aerosols and solar/viewing geometry. Thus, the relationship between $R_{rs}(\lambda)$

580   and the $R_{rc}(\lambda)$ containing various aerosols can be established through simulations. To

581   determine whether the FUI is sensitive to the considered perturbations, the FUI

582   calculated directly from $R_{rc}(\lambda)$ at MODIS RGB bands were compared with the FUI

583   calculated from the corresponding $R_{rs}(\lambda)$ with the same band setting.

584   Figure 16 shows the comparison results for maritime and coastal aerosols at the

585   scene center and scene edge. The overall relationship between R_{rs}-based FUI and R_{rc}-

586   based FUI under all light conditions is quite robust ($R^2 = 0.967$) with an MRD of 10.9%,

587   even though the relationship deteriorates a little under coastal aerosols with larger

588   aerosol optical thickness at 869 nm ($\tau(869)$) towards the scene edge. These

589   perturbations resulted in 9.5% of the data indicating a different trophic state to that

590   indicated by the FUI calculated from the original $R_{rs}(\lambda)$ data. The results illustrate that

591   the FUI algorithm is generally insensitive to perturbations due to aerosols and

592 observation conditions. This may be because of the normalization process in the

593 chromaticity coordinate calculation and the clustering process in the 21-indices

594 classification, which may reduce the uncertainties caused by different aerosol types.
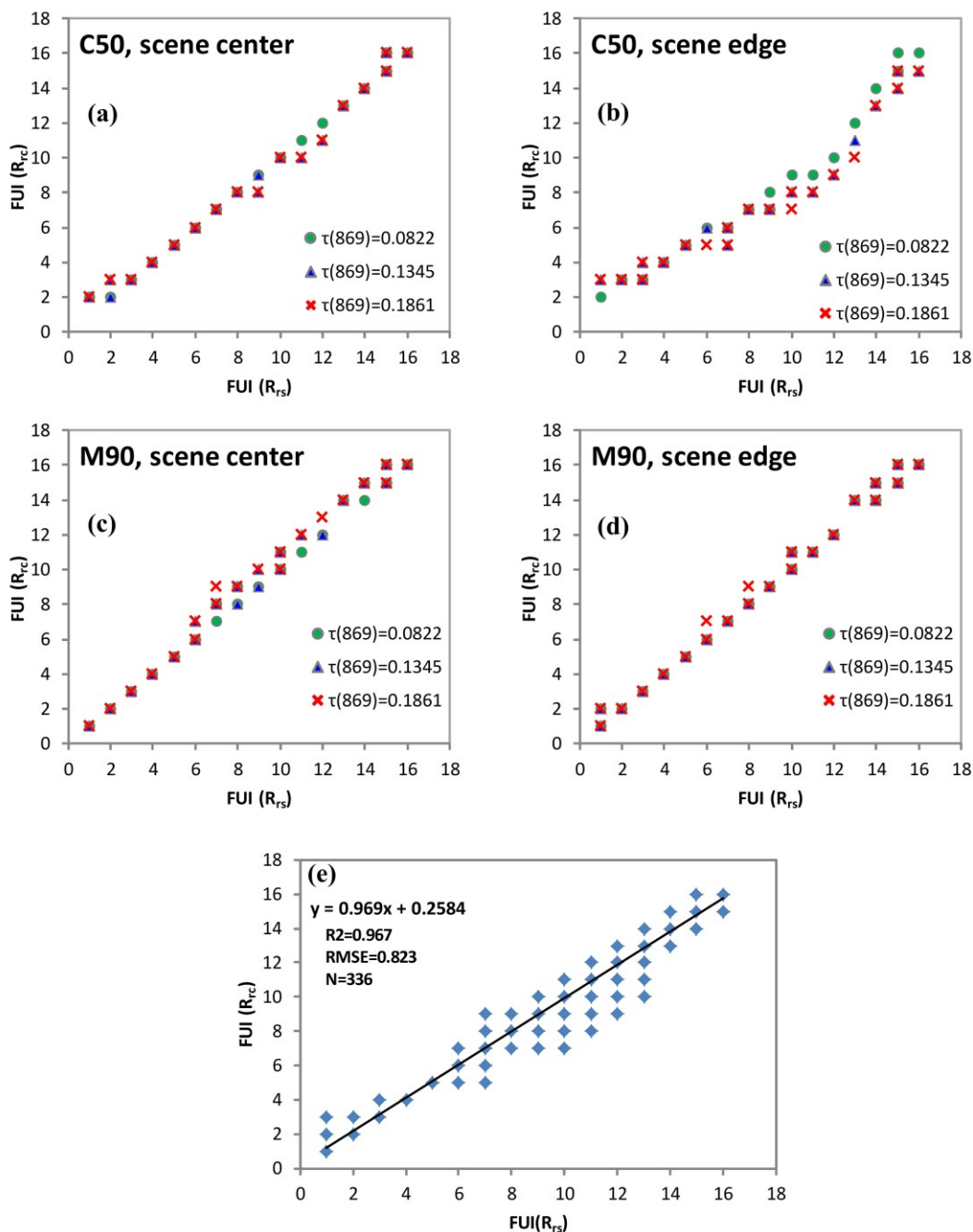
595

596 Figure 16 Relationship between R_{rc}-based FUI and R_{rs}-based FUI with various atmospheric
597 conditions (i.e., aerosol type and optical thickness at 869 nm (τ(869))) and solar/viewing geometry,
598 based on model simulations. Two aerosol types were used in the simulations: (a and b) coastal

599 aerosol with 50% relative humidity (C50) and (c and d) maritime aerosol with 90% relative humidity
600 (M90). Two solar/viewing geometries were performed in the simulations: (a and c) near scene center
601 and (b and d) near scene edge. (e) Relationship between R_{rs}-based FUI and R_{rc}-based FUI under all
602 considered conditions ($R^2 = 0.967$, MRD = 10.9%, RMSD = 0.823, n = 336). MRD denotes the
603 mean relative difference and RMSD denotes the root mean square difference.

604 **5.2 Relationship between the FUI-based method and traditional trophic state**

605 **assessments**

606   Our FUI-based trophic state assessment method depends on water colour

607 information derived from satellite imagery, which is in contrast to traditional

608 assessment methods that depend on one or several biophysical variables (i.e., Chl-a, SD,

609 TP, TN, COD and biomass; Burns et al., 1999; Vant, 1987). To compare the FUI-based

610 method with traditional variables, we compared our results with data in the NLA2007

611 report (USEPA, 2009), which contains both Chl-a based trophic state assessments, and

612 additional trophic state assessments based on SD, TP, and TN. Using the 20 lakes found

613 in both datasets, the results showed that the FUI-based classifications were better

614 correlated with SD and Chl-a ($R^2 = 0.80$, 0.65, $p < 0.05$, RD (relative error) = 30%;

615 Figure 17), reflecting the importance of water clarity and Chl-a in controlling water

616 colour. The correlation between the FUI-based results and TP-based trophic state

617 assessments was also strong ($R^2 = 0.29$, $p < 0.05$, RD = 35%). However, the TN-based

618 results had a weak relationship with the FUI-based results ($R^2 = 0.03$, RD = 55%).

619 Similarly, the TN-based results had an insignificant relationship with the Chl-a-based

620 results ($R^2 = 0.03$), as there is usually a weak relationship between TN and Chl-a in

621 lakes (Guildford and Hecky, 2000).

622   Of the 20 U.S. lakes compared, none were classified as oligotrophic in the FUI-

623   based results (Figure 17), but 5 lakes were classified as oligotrophic in the Chl-a-based

624   NLA results. This misclassification of oligotrophic lakes as mesotrophic was also seen

625   in the validation comparison data (Table 2), which will be discussed in Section 5.3.
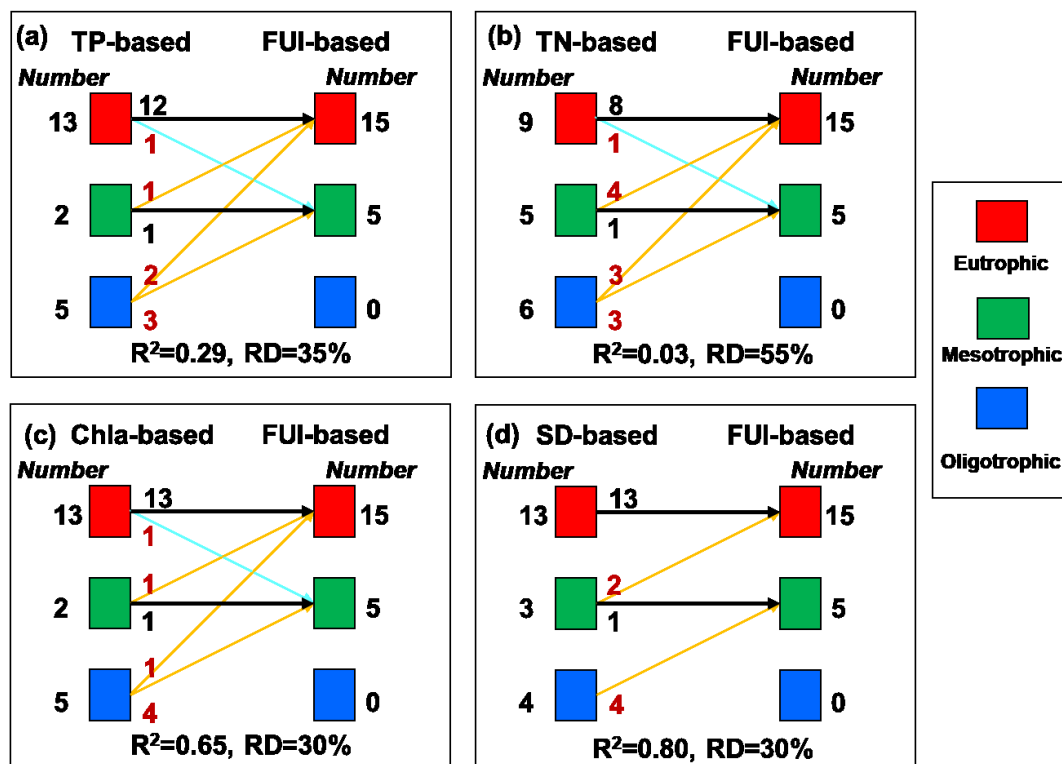
626
627   Figure 17 Comparison of lakes classified as different trophic states using the Forel-Ule index (FUI)-
628   based trophic state results and National Lake Assessment 2007 (USEPA, 2009) results based on (a)
629   total phosphorus (TP), (b) total nitrogen (TN), (c) chlorophyll-a (Chl-a), and (d) Secchi depth (SD),
630   for the 20 matched lakes. R^2 denotes the determination coefficient and RD denotes the relative error.

631   **5.3 Uncertainties of trophic state assessment using FUI**

632   Since there is currently no single RS algorithm applicable for the global inland

633   waters to retrieve the trophic state related parameters (i.e.Chl-a), as a relatively easy-

634   to-produce image product, the FUI-based method makes it possible to assess the trophic

635   states of global inland waters. Although the trophic state of the waters across the in-situ

37

636   dataset and independent dataset could be classified with relatively high accuracy (~80%)

637   with the FUI, the confusion matrix of the FUI-based classification for 100 investigated

638   lakes (Table 2) shows that the FUI method led to an over-estimation of the trophic state

639   of a small proportion of lakes. This may be explained by differences in the division of

640   the trophic states by different different assessing methods. The trophic state

641   classification in this study adopted the boundaries of 1 and 7 μg/L, based on Carlson

642   (1977). However, the USEPA (2016) adopted the boundaries of 2 and 7 μg/L. Hence,

643   there may be some over-estimation in the mesotrophic state when using the FUI method

644   because of the lower boundary. The other reason might be that the FUI of waters may

645   appear larger when there are other optically active constituents in addition to Chl-a that

646   dominate these optically complex inland waters.

647   We identified the mesotrophic waters from the eutrophic waters with FUI ≥ 10 by

648   using a red band (R_{rs}(645)) threshold method, because the relatively high CDOM

649   content in water changes the water colour to green and yellow, and the backscattering

650   of the water in the red band is quite low because of the low TSM content. In the cyan

651   box in Figure 9, there were a few other situations that result in the misclassification of

652   mesotrophic waters, which are shown in Figure 17. For these mesotrophic waters with

653   FUI ≥ 10，the optical properties are generally dominated by abundant CDOM or TSM.

654   Mesotrophic water dominated by relatively high CDOM and with very low TSM can

655   be identified from eutrophic water using the red band threshold method. However, for

656   water dominated by high CDOM with relatively high TSM, the $R_{rs}(\lambda)$ spectra is similar

657   to eutrophic waters and cannot be distinguished using the MODIS bands. It is difficult

658   to distinguish between mesotrophic and eutrophic waters when dominated by high TSM

659   with the MODIS imagery. Further assessment of the trophic state of these two specific

660   situations will require platforms with superior spectral resolution.
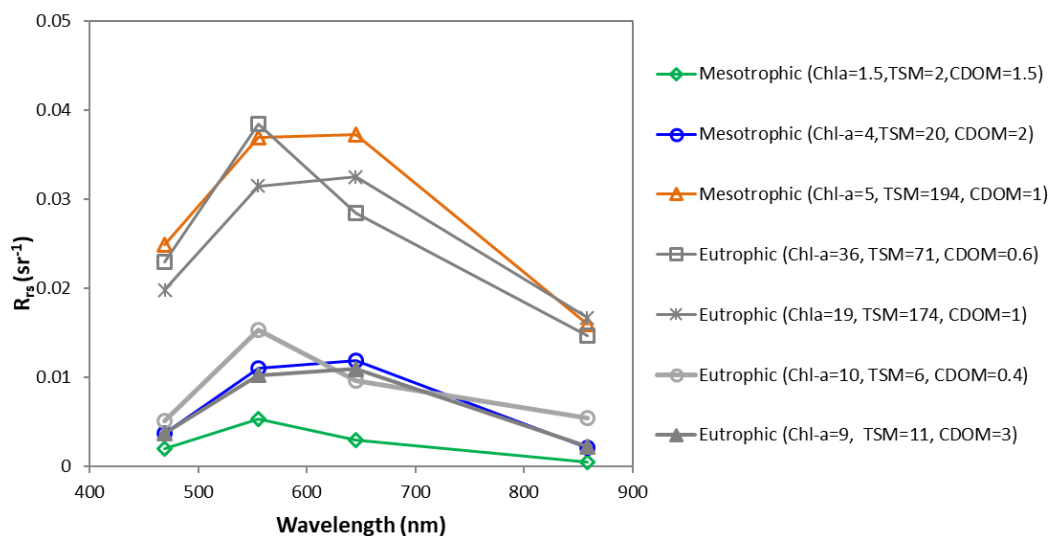
661
662   Figure 17 Different types of water-leaving reflectance ($R_{rs}(\lambda)$) spectra of waters with FUI≥10,
663   including eutrophic and confusing mesotrophic waters. The unit for Chl-a is µg/L, for TSM is
664   mg/L, for CDOM is m^{-1} which means the absorption coefficient at 440 nm.

665   As the summer-average FUI of each water body was used to assess the trophic

666   state of the water body, the averaging processes may result in the loss of spatial and

667   temporal characteristics of some water bodies, whilst reducing the occurrence of

668   unexpected errors and uncertainties. In this case, a water body that is partly eutrophic

669   and partly mesotrophic may be classified as mesotrophic after the averaging process.

670   The timing of the images also affects the results, as the trophic state of lake may change

671   during the summer months. Therefore, a threshold for the number of images of no less

672   than three over the summer months is therefore considered necessary and avoids the

673   cases where two consecutive images may produce a biased result against the average

674   state. From the global results, the spatial CV of the water bodies ranged from 0.0% to

675   41.2% with an average value of 12.9%, and the temporal CV ranged from 0.0% to 54.3%

676   with an average value of 9.9%. Large variations in these waters might in part be related

677   to the impact of cloud cover influencing or biasing the pixel coverage for a lake for

678   different areas, whilst some may also be related to extreme events such as sudden algae

679   blooms or sediment plumes following heavy rainfall.

680   The data quality of MODIS Terra was often considered not adequate for ocean

681   colour applications (Franz et al., 2008). But around 2010, NASA started reprocessing

682   of all the MODIS Terra products and produced good agreement with MODIS Aqua by

683   using improved radiometric calibration to account for sensor degradation (Li et al.,

684   2017; Lyapustin et al., 2014; Meister and Franz, 2011). In addition, for inland waters,

685   the water signal has a greater contribution in the TOA radiance, which tends to be much

686   greater than that associated with open ocean waters.

687   There may be some uncertainties induced by the calibration of Terra MODIS and

688   the artefacts of atmospheric correction in the derivation of $R_{rs}(\lambda)$ and FUI from Terra

689   MOD09 products in this study. Nevertheless, following the simple water-leaving

690   reflectance correction, the comparison between MODIS FUI and in-situ derived FUI

691   and the evaluation of the FUI sensitivity to remaining data perturbations produced good

692 results and demonstrated the validity and practicability of the MOD09 product and the

693 simple correction method for a wide range of inland waters. As might be expected, the

694 producer accuracies (Liu et al., 2007) in the confusion matrix (Table 3) for darker waters

695 like oligotrophic and mesotrophic waters, are relatively low (79.2% and 51.9%). As

696 described, this is likely associated with calibration errors and artefacts introduced from

697 atmospheric correction over dark waters (Wang et al., 2016). Hence, for global inland

698 waters with various optical properties, a more robust atmospheric correction for satellite

699 products remains a high research priority.

700 Moreover, we chose Terra MOD09 as the main data source rather than Aqua

701 MYD09 because of the frequent stripe noise. The stripe noise in band 6 (1640 nm) is

702 severe in the Aqua MYD09 and Aqua MYD02 (the Level-1B Calibrated Geolocation

703 Data Set), which is induced by the detectors in Aqua MODIS band 6 and has been

704 reported in numerous studies (Rakwatin et al., 2009; Wang et al., 2006; Doelling et al.,

705 2015). Band 6 is a useful SWIR band used in this study to detect water areas and

706 atmospheric noises; however, the stripe noise in this band in Aqua would result in

707 inaccurate water area masks and water-leaving reflectance.

708 **5.4 Applicability to new satellite sensors**

709 The FUI retrieval algorithms from the water-leaving reflectance spectra have been

710 established for various satellite sensors such as MODIS, MERIS, Landsat-8 OLI,

711 Sentinel-3 OLCI (Wang et al., 2015; Wernand et al., 2013; Van der Woerd and Wernand,

41

712 2015, 2018). There are two main approaches for calculating CIE tristimulus X, Y, Z.

713 One is to rebuild the spectral data using an interpolation approach (Van der Woerd and

714 Wernand, 2015, 2018). The other approach is specific to sensors with only RGB bands

715 in the visible range, and it converts RGB to CIE X, Y, Z using the conversion equation,

716 as shown in Equation (3) (C.I.E., 1932; Wang et al., 2015). However, despite whether

717 an interpolation approach or the RGB conversion approach is used, there would be

718 colour differences from the human eye sensed true colour caused by the band setting of

719 the sensors (Van der Woerd and Wernand, 2015). To remove this difference, a delta

720 correction method was introduced by Van der Woerd and Wernand (2015) and adopted

721 in this study which models the difference between the sensor results and the true colour

722 results using polynomial fittings. Therefore, with the delta correction, the FUI and the

723 angle α calculated can be comparable and transferable between different satellite

724 sensors (Van der Woerd and Wernand, 2015, 2018). It is notable that the definition for

725 angle α enables it increase with FUI in this study, while the definition for angle α in

726 Van der Woerd and Wernand (2015) results in a decrease with FUI considering the

727 different start and revolving direction of angle α adopted. A transfer is first required

728 when comparing angle α derived using the different definitions. Regardless of the

729 definition of angle α, the FUI calculated are consistent because the same set of

730 chromaticity coordinates of the Forel-Ule scales were used (Novoa et al., 2013).

731 Furthermore, the FUI calculated from new sensors, like Landsat-8 OLI and Sentinel-3

732 OLCI, could be generally comparable with that from MODIS using a proper correction

733 method for the band settings (Van der Woerd and Wernand, 2018). With recently

734 launched sensors such as the Landsat-8 OLI and Sentinel-2(A & B), smaller lakes can

735 be added to the dataset to achieve more comprehensive global results.

6. Conclusions

737   In this study, the trophic states of global large inland waters were assessed using

738 an FUI-based remote sensing algorithm. The successful outcome can be attributed to

739 two factors: (1) the water colour index, FUI, can be calculated from MOD09A1 data

740 with considerable accuracy (~90%) through comparison with in-situ data, and it is

741 nearly immune to aerosol perturbations and variations in observation conditions. Such

742 tolerances lead to significantly increased validity, which is critical to FUI's application

743 on the global scale; (2) The FUI-based trophic state assessment algorithm was

744 developed based on the analysis of the relationship between FUI and TSI from 469

745 samples from in-situ measurements at 10 lakes around the world, which contain a wide

746 range of optical and water quality properties. This led to a robust trophic state

747 assessment method for inland waters on large scales, and an overall accuracy of 80%

748 was achieved. This algorithm could be applied to other satellite sensors with the

749 establishment of FUI retrieval algorithms from various sensors.

750   The assessment algorithm was implemented on MODIS images collected in the

751 austral and boreal summers of 2012, and the trophic states of the water bodies were

752 classified as oligotrophic, mesotrophic, or eutrophic. Of the 2058 water bodies

753 considered, eutrophic water bodies accounted for 63.1% of the total number but only

754 30.5% of the total surface area, mesotrophic water bodies accounted for 26.2% of the

755 total number and 39.4% of the total surface area, and oligotrophic water bodies

756 accounted for 10.7% of the total number but 30.1% of the total surface area.

757 Oligotrophic large lakes were found to be concentrated in plateau regions in Central

758 Asia and southern South America, while eutrophic large lakes were concentrated in

759 central Africa, eastern Asia, and mid-northern and southeast North America.

References

770 Auer, M. T., Bub, L. A. (2004). Selected features of the distribution of chlorophyll along
771 the southern shore of Lake Superior. Journal of Great Lakes Research, 30, 269-284.
772 Avery, S., Eng, C. (2012). Lake Turkana & the Lower Omo: hydrological impacts of
773 major dam and irrigation developments. African Studies Centre, the University of

774   Oxford.

775   Baban, S. M. (1996). Trophic classification and ecosystem checking of lakes using
776   remotely sensed information. Hydrological sciences journal, 41(6), 939-957.

777   Barbiero, R. P., Lesht, B. M., Warren, G. J. (2012). Convergence of trophic state and
778   the lower food web in lakes huron, michigan and superior. Journal of Great Lakes
779   Research, 38(2), 368-380.

780   Beeton, A. M., Edmondson, W. T. (1972). The eutrophication problem. Journal of the
781   Fisheries Board of Canada, 29(6), 673-682.

782   Bigham Stephens, D. L., Carlson, R. E., Horsburgh, C. A., Hoyer, M. V., Bachmann, R.
783   W., Canfield Jr, D. E. (2015). Regional distribution of Secchi disk transparency in
784   waters of the United States. Lake and Reservoir Management, 31(1), 55-63.

785   Binding, C. E., Greenberg, T. A., Watson, S. B., Rastin, S., Gould, J. (2015). Long term
786   water clarity changes in North America's Great Lakes from multi-sensor satellite
787   observations.   Limnology   and   Oceanography,   60(6),   1976-1995.
788   http://doi.org/10.1002/lno.10146.

789   Binding, C. E., T. A. Greenberg, and R. P. Bukata. (2013). The MERIS Maximum
790   Chlorophyll Index; its merits and limitations for inland water algal bloom
791   monitoring. J. Great Lakes Res. 39: 100–107. doi:10.1016/j.jglr.2013.04.005

792   Bridgeman, T. B., Chaffin, J. D., Filbrun, J. E. (2013). A novel method for tracking
793   western Lake Erie Microcystis blooms, 2002–2011. Journal of Great Lakes
794   Research, 39(1), 83-89.

795   Bukata, P. R., Jerome, J. H., Kondratyev, K. Y., Pozdnyakov, D. (1995). Optical
796   Properties and Remote Sensing of Inland and Coastal Waters Boca Raton: CRC
797   Press.

798   Bukata, R. P., Bruton, J. E., Jerome, J. H. (1983). Use of chromaticity in remote
799   measurements of water-quality. Remote Sensing of Environment, 13(2), 161-177.

800   Burns, N. M., Bryers, G. (2000). Protocols for monitoring trophic levels of New
801   Zealand lakes and reservoirs. Ministry for the Environment.

802   Burns, N. M., Rutherford, J. C., Clayton, J. S. (1999). A monitoring and classification
803   system for New Zealand lakes and reservoirs. Lake and Reservoir Management,
804   15(4), 255-271.

805   C.I.E. (1932). Commission Internationale de l'Eclairage Proceedings 1931, Cambridge
806   Univ. Press, 19-29.

807   Carlson, R. E. (1977). A trophic state index for lakes. Limnology and oceanography,
808   22(2), 361-369.

809   Carlson, R. E. (1991). Expanding the trophic state concept to identify non-nutrient
810   limited lakes and reservoirs. Enhancing the states's lake management programs,
811   59-71.

812   Chaffin, J. D., Bridgeman, T. B., Heckathorn, S. A., Mishra, S. (2011). Assessment of
813   Microcystis growth rate potential and nutrient status across a trophic gradient in
814   western Lake Erie. Journal of Great Lakes Research, 37(1), 92-100.

815   Chen, J., Quan, W., Zhang, M., Cui, T. (2013a). A simple atmospheric correction
816   algorithm for MODIS in shallow turbid waters: A case study in Taihu Lake. IEEE
817   Journal of Selected Topics in Applied Earth Observations and Remote Sensing,
818   6(4), 1825-1833.
819   Chen, L. (2003). A study of applying genetic programming to reservoir trophic state
820   evaluation using remote sensor data. International Journal of Remote Sensing,
821   24(11), 2265-2275.
822   Chen, R. (2009). Research on water quality appraisal and water environmental capacity
823   of Zhelin Reservoir. Master Dissertation. Nanchang University.
824   Chen, X., Yang, X., Dong, X., Liu, E. (2013b). Environmental changes in Chaohu Lake
825   (southeast, China) since the mid-20th century: the interactive impacts of nutrients,
826   hydrology and climate. Limnologica-Ecology and Management of Inland Waters,
827   43(1), 10-17.
828   Cheng, K. S., Lei, T. C. (2001). Reservoir trophic state evaluation using Landsat TM
829   images. Journal of the American Water Resources Association, 37, 1321-1334.
830   Chernetskiy, M., Shevyrnogov, A., Shevnina, S., Vysotskaya, G., Sidko, A. (2009).
831   Investigations of the Krasnoyarsk Reservoir waters based on the multispectral
832   satellite data. Advances in Space Research, 43(2), 206-213.
833   Coci, M., Odermatt, N., Salcher, M. M., Pernthaler, J., Corno, G. (2015). Ecology and
834   distribution of thaumarchaea in the deep hypolimnion of Lake Maggiore. Archaea-
835   an International Microbiological Journal, 2015.
836   Diaz, M., Pedrozo, F. and Baccala, N. (2000). Summer classification of Southern
837   Hemisphere temperate lakes (Patagonia, Argentina). Lakes & Reservoirs: Research
838   & Management, 5: 213–229.
839   Dierssen, H.M., Zimmerman, R.C., Leathers, R.A., Downes, T.V. and Davis, C.O., 2003.
840   Ocean color remote sensing of seagrass and bathymetry in the Bahamas Banks by
841   high‐resolution airborne imagery. Limnology and oceanography, 48(1part2),
842   pp.444-455.
843   Doelling, D. R., Wu, A., Xiong, X., Scarino, B. R., Bhatt, R., Haney, C. O., Gopalan,
844   A. (2015). The radiometric stability and scaling of collection 6 Terra-and Aqua-
845   MODIS VIS, NIR, and SWIR spectral bands. IEEE Transactions on Geoscience
846   and Remote Sensing, 53(8), 4520-4535.
847   Duan, H., Zhang, Y., Zhang, B., Song, K., Wang, Z. (2007). Assessment of chlorophyll-
848   a concentration and trophic state for Lake Chagan using Landsat TM and field
849   spectral data. Environmental monitoring and assessment, 129(1-3), 295-308.
850   Fitzsimmons, K. E., Barrows, T. T. (2010). Holocene hydrologic variability in
851   temperate southeastern Australia: an example from Lake George, New South Wales.
852   The Holocene, 20(4), 585-597.
853   Forsberg, D., Ryding, S. O. (1980). Eutrophication parameters and trophic indices in
854   30 Swedish lakes. Arch Hydrobiol.89:189–207.
855   Friedl, M. A., Sulla-Menashe, D., Tan, B., Schneider, A., Ramankutty, N., Sibley, A.,

856   andHuang, X. (2010). MODIS Collection 5 global land cover: Algorithm
857   refinements and characterization of new datasets. Remote Sensing of Environment,
858   114, 168–182.
859   Fuentes, N., Güde, H., Wessels, M., Straile, D. (2013). Allochthonous contribution to
860   seasonal and spatial variability of organic matter sedimentation in a deep
861   oligotrophic lake (Lake Constance). Limnologica-Ecology and Management of
862   Inland Waters, 43(2), 122-130.
863   Garaba, S. P., Badewien, T. H., Braun, A., Schulz, A.-C., Zielinski, O. (2014). Using
864   ocean colour remote sensing products to estimate turbidity at the Wadden Sea time
865   series station Spiekeroog. J. Europ. Opt. Soc. Rap. Public. 9 (14020): 1-6.
866   Giardino, C., Bresciani, M., Stroppiana, D., Oggioni, A., Morabito, G. (2013). Optical
867   remote sensing of lakes: an overview on Lake Maggiore. Journal of Limnology,
868   73(s1).
869   Giardino, C., Bresciani, M., Cazzaniga, I., Schenk, K., Rieger, P., Braga, F., et al. (2014).
870   Evaluation of multi-resolution satellite sensors for assessing water quality and
871   bottom depth of lake garda. Sensors, 14(12), 24116-31
872   Guildford, S.J. and Hecky, R.E., (2000). Total nitrogen, total phosphorus, and nutrient
873   limitation in lakes and oceans: is there a common relationship?. Limnology and
874   Oceanography, 45(6), 1213-1223.
875   Härmä, P., Vepsäläinen, J., Hannonen, T., Pyhälahti, T., Kämäri, J., Kallio, K. (2001).
876   Detection of water quality using simulated satellite data and semi-empirical
877   algorithms in Finland. Science of the Total Environment, 268(1), 107-121.
878   Hecky, R. E., Mugidde, R., Ramlal, P. S., Talbot, M. R., Kling, G. W. (2010). Multiple
879   stressors cause rapid ecosystem change in Lake Victoria. Freshwater Biology,
880   55(s1), 19-42.
881   Holden, H., LeDrew, E. (2002). Measuring and modeling water column effects on
882   hyperspectral reflectance in a coral reef environment. Remote Sensing of
883   Environment, 81(2), 300-308.
884   Holeck, K. T., Rudstam, L. G., Watkins, J. M., Luckey, F. J., Lantry, J. R., Lantry, B. F.,
885   Johnson, T. B. (2015). Lake Ontario water quality during the 2003 and 2008
886   intensive field years and comparison with long-term trends. Aquatic Ecosystem
887   Health & Management, 18(1), 7-17.
888   Hou, X., Feng, L., Duan, H., Chen, X., Sun, D., Shi, K. (2017). Fifteen-year monitoring
889   of the turbidity dynamics in large lakes and reservoirs in the middle and lower basin
890   of the Yangtze River, China. Remote Sensing of Environment, 190, 107-121.
891   Hu, C., K. L. Carder, and F. E. Muller-Karger. (2000). Atmospheric Correction of
892   SeaWiFS Imagery over Turbid Coastal Waters: A Practical Method. Remote
893   Sensing of Environment 74: 195–206. doi:10.1016/S0034-4257(00)00080-8.
894   Hu, C., Lee, Z., Ma, R., Yu, K., Li, D., Shang, S. (2010). Moderate resolution imaging
895   spectroradiometer (MODIS) observations of cyanobacteria blooms in Taihu Lake,
896   China. Journal of Geophysical Research: Oceans, 115(C4).

47

897 Hurlbert, S. H. (Ed.). (2012). Saline Lakes V: Proceedings of the Vth International
898   Symposium on Inland Saline Lakes, held in Bolivia, 22–29 March 1991 (Vol. 87).
899   Springer Science & Business Media.

900 IOCCG (2006). Remote sensing of Inherent Optical Properties: fundamentals, tests of
901   algorithms, and applications. Lee, Z.-P. (ed.), Reports of the International Ocean-
902   Colour Coordinating Group, No. 5, IOCCG, Dartmouth, Canada.

903 Jacobs L L. (1989). Limnological characteristics of big and litile minto lakes, Alaska.
904   Alaska's hidden resource, 1989: 17.

905 Jaquet, J. M., Nirel, P., Martignier, A. (2013). Preliminary investigations on
906   picoplankton-related precipitation of alkaline-earth metal carbonates in meso-
907   oligotrophic Lake Geneva (Switzerland). Journal of Limnology, 72(3), 50.

908 Jin, X. C., Tu, Q. Y. (1990). The standard methods for observation and analysis in lake
909   eutrophication. Chinese Environmental Science Press, Beijing, 240.

910 Jones, R. A., Lee, G. F. (1982). Recent advances in assessing impact of phosphorus
911   loads on eutrophication-related water quality. Water Research, 16(5), 503-515.

912 Joniak, T., Nagengast, B., Kuczynska-Kippin, N. (2009). Can popular systems of
913   trophic classified be used for small water bodies? Oceanological and
914   hydrobiological studies. International Journal of oceanography and hydrobiology,
915   XXXVIII(4), 145–151

916 Khandelwal, A., Karpatne, A., Marlier, M. E., Kim, J., Lettenmaier, D. P., Kumar, V.
917   (2017). An approach for global monitoring of surface water extent variations in
918   reservoirs using MODIS data. Remote Sensing of Environment.

919 Kingston, John. (2015). Completion Report Mille Lacs Lake Paleolimnology Project.
920   http://hdl.handle.net/10792/1832.

921 Klein, I., Gessner, U., Dietz, A. J., Kuenzer, C. (2017). Global WaterPack–A 250 m
922   resolution dataset revealing the daily dynamics of global inland water bodies.
923   Remote Sensing of Environment, 198, 345-362.

924 Knight, J. F., Voth, M. L. (2012). Application of MODIS imagery for intra-annual water
925   clarity assessment of Minnesota lakes. Remote Sensing, 4(7), 2181-2198.

926 Kshitij Mishra and P. Rama Chandra Prasad. (2015). Automatic extraction of water
927   bodies from Landsat imagery using Perceptron model, Journal of Computational
928   Environmental Sciences, vol. 2015, Article ID 903465, 9 pages, 2015.
929   doi:10.1155/2015/903465

930 Kutser, T., E. Vahtm€ae, B. Paavel, and T. Kauer. (2013). Removing glint effects from
931   field radiometry data measured in optically complex coastal and inland waters.
932   Remote Sens. Environ. 133: 85–89. doi:10.1016/j.rse.2013.02.011

933 Landis, J. R., Koch, G. G. (1977). An application of hierarchical kappa-type statistics
934   in the assessment of majority agreement among multiple observers. Biometrics,
935   363-374.

936 Le, C., Zha, Y., Li, Y., Sun, D., Lu, H., Yin, B. (2010). Eutrophication of lake waters in
937   China: cost, causes, and control. Environmental Management, 45(4), 662-668.

938 Lee, Z., Carder, K. L., Mobley, C. D., Steward, R. G., Patch, J. S. (1998). Hyperspectral
939   remote sensing for shallow waters. I. A semianalytical model. Applied optics,
940   37(27), 6329-6338.
941 Lehner, B., Döll, P. (2004). Global Lakes and Wetlands Database GLWD. GLWD Docu
942   mentation.
943 Li J., Wu D., Wu Y., Liu H., Shen Q., Zhang H. (2009). Identification of algae-bloom
944   and aquatic macrophytes in Lake Taihu from in-situ measured spectra data. Journal
945   of Lake Sciences, 21(2), 215-222.
946 Li, J., Wang, S., Wu, Y., Zhang, B., Chen, X., Zhang, F., Shen, Q., Peng, D., Tian, L.
947   (2016). MODIS observations of water color of the largest ten lakes in China
948   between 2000 and 2012. International Journal of Digital Earth, 1-18.
949 Lillesand, T. M., Johnson, W. L., Deuell, R. L., Lindstrom, O. M., Meisner, D. E. (1983).
950   Use of Landsat data to predict the trophic state of Minnesota lakes.
951 Lim, A., Hedley, J. D., LeDrew, E., Mumby, P. J., Roelfsema, C. (2009). The effects of
952   ecologically determined spatial complexity on the classification accuracy of
953   simulated coral reef images. Remote Sensing of Environment, 113(5), 965-978.
954 Liu, C., Frazier, P., Kumar, L. (2007). Comparative assessment of the measures of
955   thematic classification accuracy. Remote sensing of environment, 107(4), 606-616.
956 Lyzenga, D. R. (1978). Passive remote sensing techniques for mapping water depth and
957   bottom features. Applied optics, 17(3), 379-383.
958 Ma, S., Tao, Z., Yang, X., Yu, Y., Zhou, X., Li, Z. (2014). Bathymetry retrieval from
959   hyperspectral remote sensing data in optical-shallow water. IEEE Transactions on
960   Geoscience and Remote Sensing, 52(2), 1205-1212.
961 Matthews, M. W., Odermatt, D. (2015). Improved algorithm for routine monitoring of
962   cyanobacteria and eutrophication in inland and near-coastal waters. Remote
963   Sensing of Environment, 156, 374-382.
964 McClain, C. R. (2009). A decade of satellite ocean color observations*. Annual Review
965   of Marine Science, 1, 19-42.
966 Ministry of Environmental Protection of the People's Republic of China (MEPPRC).
967   2013.   China   Environmental   State   Bulletin   2012.
968   http://jcs.mep.gov.cn/hjzl/zkgb/2012zkgb/.
969 Mobley, C. D., Sundman, L. K. (2003). Effects of optically shallow bottoms on
970   upwelling radiances: Inhomogeneous and sloping bottoms. Limnology and
971   Oceanography, 48(1part2), 329-336.
972 Mukherjee, M., Ray, A., Post, A. F., McKay, R. M., Bullerjahn, G. S. (2016).
973   Identification, enumeration and diversity of nitrifying planktonic archaea and
974   bacteria in trophic end members of the Laurentian Great Lakes. Journal of Great
975   Lakes Research, 42(1), 39-49.
976 Okullo, W., Hamre, B., Frette, Ø, Stamnes, J. J., Sørensen, K., Ssenyonga, T. (2011).
977   Validation of MERIS water quality products in Murchison bay, Lake Victoria–
978   preliminary results. International journal of remote sensing, 32(19), 5541-5563.

979 Olmanson, L. G., Bauer, M. E., Brezonik, P. L. (2008). A 20-year Landsat water clarity
980   census of Minnesota's 10,000 lakes. Remote Sensing of Environment, 112(11),
981   4086-4097.

982 O'Reilly, C. M., Alin, S. R., Plisnier, P. D., Cohen, A. S., McKee, B. A. (2003). Climate
983   change decreases aquatic ecosystem productivity of Lake Tanganyika, Africa.
984   Nature, 424(6950), 766-768.

985 O'Reilly, J.E., Maritorena, S., Mitchell, B. G., Siegel, D. A., Carder, K. L., Garver, S.
986   A., Kahru, M., McClain, C. R. (1998). Ocean color chlorophyll algorithms for
987   SeaWiFS, Journal of Geophysical Research 103, 24937-24953, doi:
988   10.1029/98JC02160.

989 Palmer, S. C. J., Kutser, T., Hunter, P. D. (2015). Remote sensing of inland waters:
990   Challenges, progress and future directions. Remote Sensing of Environment, 157,
991   1-8. doi:10.1016/j.rse.2014.09.021

992 Papoutsa, C., Akylas, E., Hadjimitsis, D. (2014). Trophic State Index derivation through
993   the remote sensing of Case-2 water bodies in the Mediterranean Region. Open
994   Geosciences, 6(1), 67-78.

995 Pulliainen, J., Kallio, K., Eloheimo, K., Koponen, S., Servomaa, H., et al. (2001). A
996   semi-operative approach to lake water quality retrieval from remote sensing data.
997   Science of the Total Environment, 268(1), 79-93.

998 Raji, A. (1993). The past history and present trends in the fisheries of Lake Chad. 213-
999   225.

1000 Rakwatin, P., Takeuchi, W., Yasuoka, Y. (2009). Restoration of Aqua MODIS band 6
1001   using histogram matching and local least squares fitting. IEEE Transactions on
1002   Geoscience and Remote Sensing, 47(2), 613-627.

1003 Rimet, F., Bouchez, A., Montuelle, B. (2015). Benthic diatoms and phytoplankton to
1004   assess nutrients in a large lake: Complementarity of their use in Lake Geneva
1005   (France–Switzerland). Ecological Indicators, 53, 231-239.

1006 Rodhe, W. (1969). Crystallization of eutrophication concepts in northern Europe.

1007 Sass, G. Z., Creed, I. F., Bayley, S. E., Devito, K. J. (2007). Understanding variation in
1008   trophic status of lakes on the Boreal Plain: a 20 year retrospective using Landsat
1009   TM imagery. Remote Sensing of Environment, 109(2), 127-141.

1010 Shanmugam, P., Ahn, Y. (2007). New Atmospheric Correction Technique to Retrieve
1011   the Ocean Colour from Seawifs Imagery in Complexcoastal Waters. Journal of
1012   Optics A: Pure and Applied Optics 9: 511–530. doi:10.1088/1464-4258/9/5/016.

1013 Sheela, A. M., Letha, J., Joseph, S. (2011b). Environmental status of a tropical lake
1014   system. Environmental monitoring and assessment, 180(1-4), 427-449.

1015 Sheela, A. M., Letha, J., Joseph, S., Ramachandran, K. K., Sanalkumar, S. P. (2011a).
1016   Trophic state index of a lake system using IRS (P6-LISS III) satellite imagery.
1017   Environmental monitoring and assessment, 177(1-4), 575-592.

1018 Shen, Q., Li, J. S., Wu, Y. H., Zhang, B. (2014). Review of spectral curve fitting and
1019   analysis of inherent optical parameters in lakes. Remote Sensing Information, 29

1020 (4): 112-125.

1021 Sheng, H.，Wu, Z., Liu, M., et al. (2015). Water quality trends in recent 10 years and
1022 correlation with hydro-meteorological factors in Xin'anjiang Reservoir．Acta
1023 Scientiae Circumstantiae, 35(1): 118-127.

1024 Shi, K., Zhang, Y., Zhu, G., Liu, X., Zhou, Y., Xu, H., et al. (2015). Long-term remote
1025 monitoring of total suspended matter concentration in Lake Taihu using 250m
1026 MODIS-Aqua data. Remote Sensing of Environment, 164, 43-56.

1027 Shi, W., Wang M. (2009). An assessment of the black ocean pixel assumption for
1028 MODIS SWIR bands. Remote sensing of environment 113(8): 1587-1597.

1029 Shuchman, R. A., Leshkevich, G., Sayers, M. J., Johengen, T. H., Brooks, C. N.,
1030 Pozdnyakov, D. (2013). An algorithm to retrieve chlorophyll, dissolved organic
1031 carbon, and suspended minerals from Great Lakes satellite data. Journal of Great
1032 Lakes Research, 39, 14-33.

1033 Singh, S.P. and Singh, P. (2015). Effect of temperature and light on the growth of algae
1034 species: a review. Renewable and Sustainable Energy Reviews, 50, pp.431-444.

1035 Smith, V. H. (2003). Eutrophication of freshwater and coastal marine ecosystems a
1036 global problem. Environmental Science and Pollution Research, 10(2): 126-139.

1037 Song, K., Ma, J., Wen, Z., Fang, C., Shang, Y., Zhao, Y., Du, J. (2017). Remote
1038 estimation of K d (PAR) using MODIS and Landsat imagery for turbid inland
1039 waters in Northeast China. ISPRS Journal of Photogrammetry and Remote Sensing,
1040 123, 159-172.

1041 Spyrakos, E., O'Donnell, R., Hunter, P.D., Miller, C., Scott, M., Simis, S.G., Neil, C.,
1042 Barbosa, C.C., Binding, C.E., Bradt, S. and Bresciani, M. (2018). Optical types of
1043 inland and coastal waters. Limnology and Oceanography, 63(2), pp.846-870.

1044 Stich, H. B., Brinker, A. (2010). Oligotrophication outweighs effects of global warming
1045 in a large, deep, stratified lake ecosystem. Global Change Biology, 16(2), 877-888.

1046 Strahler, A., Muchoney, D., Borak, J., Friedl, M., Gopal, S., Lambin, E., Moody, A.,
1047 (1999). MODIS Land Cover Product: Algorithm Theoretical Basis Document
1048 (ATBD), Version 5.0. Boston University, Boston, MA, 72 p.

1049 Stuart H. Hurlbert. (1991).Saline Lakes V, Proceedings of the Vth International
1050 Symposium on Inland Saline Lakes, held in Bolivia, 22–29 March 1991.

1051 Tang, J. W., Tian, G. L., Wang, X. Y., Wang, X. M., Song, Q. J. (2004). The methods of
1052 water spectra measurement and analysis I: above-water method. Journal of Remote
1053 Sensing, 8(1), 37-44.

1054 Thiemann, S., Kaufmann, H. (2000). Determination of chlorophyll content and trophic
1055 state of lakes using field spectrometer and IRS-1C satellite data in the Mecklenburg
1056 Lake District, Germany. Remote Sensing of Environment, 73(2), 227-235.

1057 USEPA. (2009). National Lakes Assessment: A collaborative survey of the Nation's
1058 Lakes. EPA 841-R-09-001. U.S. Environmental Protection Agency, Office of Water
1059 and Office of Research and Development, Washington, D.C.
1060 https://nationallakesassessment.epa.gov/

1061   USEPA. (2016). National Lakes Assessment 2012: A collaborative survey of lakes in
1062   the United States. EPA 841-R-16-113. U.S. Environmental Protection Agency,
1063   Washington, DC. https://nationallakesassessment.epa.gov/

1064   Vant, W. N. (Ed.). (1987). Lake managers handbook: a guide to undertaking and
1065   understanding investigations into lake ecosystems, so as to assess management
1066   options for lakes (No. 103). Published for the National Water and Soil Conservation
1067   Authority by the Water and Soil Directorate, Ministry of Works and Development.

1068   Velpuri, N. M., Senay, G. B., Asante, K. O. (2012). A multi-source satellite data
1069   approach for modelling Lake Turkana water level: calibration and validation using
1070   satellite altimetry data. Hydrology and Earth System Sciences, 16(1), 1-18.

1071   Verburg, P. (2006). The need to correct for the Suess effect in the application of δ13C
1072   in sediment of autotrophic Lake Tanganyika, as a productivity proxy in the
1073   Anthropocene. Journal of Paleolimnology, 37(4): 591-602.

1074   Verburg, P., Hamill, K., Unwin, M., Abell, J. (2010). Lake water quality in New Zealand
1075   2010: Status and trends. NIWA client report HAM, 107.

1076   Vermote, E., Vermeulen A. (1999). Atmospheric correction algorithm: spectral
1077   reflectances (MOD09), ATBD version 4. https://eospso.gsfc.nasa.gov/sites/
1078   default/files/atbd/atbd_mod08.pdf. (Accessed April 1999).

1079   Vermote, E. F., Roger, J. C., Ray, J. P. (2015). MODIS Surface Reflectance User's
1080   Guide-Collection 6. In Tech. Rep. Version 1.4, NASA GSFC Terrestrial
1081   Information Systems Laboratory, MODIS Land Surface Reflectance Science
1082   Computing Facility. Greenbelt, USA.

1083   Vollenweider, R. A. (1981). Eutrophication- a Global Problem. Water Qual. Bull., 6(3),
1084   59-62.

1085   Vollenweider, R. A., Kerekes, J. (1982). Eutrophication of waters. Monitoring,
1086   assessment and control. Organization for Economic Co-Operation and
1087   Development (OECD), Paris, 156.

1088   Wang, L., Qu, J. J., Xiong, X., Hao, X., Xie, Y., Che, N. (2006). A new method for
1089   retrieving band 6 of Aqua MODIS. IEEE Geoscience and Remote Sensing Letters,
1090   3(2), 267-270.

1091   Wang, M., and W. Shi. (2007).The NIR-SWIR Combined Atmospheric Correction
1092   Approach for MODIS Ocean Color Data Processing. Optics Express 15: 15722–
1093   15733. doi:10.1364/OE.15.015722.

1094   Wang, M., Shi, W., Tang, J. (2011). Water property monitoring and assessment for
1095   China's inland Lake Taihu from MODIS-Aqua measurements. Remote Sensing of
1096   Environment, 115(3), 841-854.

1097   Wang, S. M., Dou, H. S. (1998). Chinese Lakes. Science Press, Beijing.

1098   Wang, S., Li, J., Shen, Q., Zhang, B., Zhang, F., Lu, Z. (2015). MODIS-based
1099   radiometric color extraction and classification of inland water with the Forel-Ule
1100   Scale: A Case Study of Lake Taihu. IEEE Journal of Selected Topics in Applied
1101   Earth Observations and Remote Sensing, 8(2), 907-918.

1102 Wang. S., Li, J., Zhang, B., Shen, Q., Zhang, F., Lu, Z. (2016). A simple correction
1103   method for the MODIS surface reflectance product over typical inland waters in
1104   China, International Journal of Remote Sensing, 37:24, 6076-6096.

1105 Wang, Z., Hong, J., Du, G. (2008). Use of satellite imagery to assess the trophic state
1106   of Miyun Reservoir, Beijing, China. Environmental Pollution, 155(1), 13-19.

1107 Wernand, M. R., Van der Woerd, H. J. (2010). Spectral analysis of the Forel-Ule Ocean
1108   colour comparator scale. Journal of the European Optical Society-Rapid
1109   Publications, 5.

1110 Wernand, M. R., Hommersom, A., Van der Woerd, H. J. (2013a). MERIS-based ocean
1111   colour classification with the discrete Forel-Ule scale. Ocean Science 9: 477-487.

1112 Wernand, M.R., Van der Woerd, H.J., Gieskes, W.W.C. (2013b). Trends in Ocean
1113   Colour and Chlorophyll Concentration from 1889 to 2000, Worldwide. PLoS ONE
1114   8(6): e63766. doi:10.1371/journal.pone.0063766

1115 Williams, W. (2002). Environmental threats to salt lakes and the likely status of inland
1116   saline ecosystems in 2025. Environmental Conservation, 29(2), 154-167.
1117   doi:10.1017/S0376892902000103

1118 Van der Woerd, H. J., Wernand, M. R. (2015). True colour classification of natural
1119   waters with medium-spectral resolution satellites: SeaWiFS, MODIS, MERIS and
1120   OLCI. Sensors, 15(10), 25663-25680.

1121 Van der Woerd H.J. et al., (2016).True color analysis of natural waters with SeaWiFS,
1122   MODIS, MERIS and OLCI by SNAP. Presented at Ocean Optics conference, At
1123   Victoria BC Canada, Volume: XXIII.

1124 Wu, G., Cui, L., He, J., Duan, H., Fei, T., Liu, Y. (2013). Comparison of MODIS-based
1125   models for retrieving suspended particulate matter concentrations in Poyang Lake,
1126   China. International Journal of Applied Earth Observation and Geoinformation, 24,
1127   63-72.

1128 Wu, G., De Leeuw, J., Skidmore, A. K., Prins, H. H., Liu, Y. (2008). Comparison of
1129   MODIS and Landsat TM5 images for mapping tempo–spatial dynamics of Secchi
1130   disk depths in Poyang Lake National Nature Reserve, China. International Journal
1131   of Remote Sensing, 29(8), 2183-2198.

1132 Xiang, B., Song, J. W., Wang, X. Y., Zhen, J. (2015). Improving the accuracy of
1133   estimation of eutrophication state index using a remote sensing data-driven method:
1134   A case study of Chaohu Lake, China. Water SA, 41(5), 753-761.

1135 Yang, L., Lei, K., Meng, W., Fu, G., Yan, W. (2013). Temporal and spatial changes in
1136   nutrients and chlorophyll-α in a shallow lake, Lake Chaohu, China: An 11-year
1137   investigation. Journal of Environmental Sciences, 25(6), 1117-1123.

1138 Ylöstalo, P., Kallio, K., Seppälä, J. (2014). Absorption properties of in-water
1139   constituents and their variation among various lake types in the boreal region.
1140   Remote Sensing of Environment, 148, 190-205.

1141 Zhang, F., Li, J., Zhang, B., Shen, Q., Ye, H., Wang, S., Lu, Z. (2018). A simple
1142   automated dynamic threshold extraction method for the classification of large

1143 water bodies from landsat-8 OLI water index images. International Journal of
1144 Remote Sensing, 39(11), 3429-3451.

1145 Zhang, M., R. Ma, J. Li, B. Zhang, and H. Duan. (2014). A Validation Study of an
1146 Improved SWIR Iterative Atmospheric Correction Algorithm for MODIS-Aqua
1147 Measurements in Lake Taihu, China. IEEE Transactions on Geoscience and
1148 Remote Sensing 52 (8): 4686–4695. doi:10.1109/TGRS.2013.2283523.